Multimedia Contents

69. Physical Human–Robot Interaction

Sami Haddadin, Elizabeth Croft

Over the last two decades, the foundations for physical human–robot interaction (pHRI) have evolved from successful developments in mechatronics, control, and planning, leading toward safer lightweight robot designs and interaction control schemes that advance beyond the current capacities of existing high-payload and high-precision position-controlled industrial robots. Based on their ability to sense physical interaction, render compliant behavior along the robot structure, plan motions that respect human preferences, and generate interaction plans for collaboration and coaction with humans, these novel robots have opened up novel and unforeseen application domains, and have advanced the field of human safety in robotics.

This chapter gives an overview on the state of the art in pHRI. First, the advances in human safety are outlined, addressing topics in human injury analysis in robotics and safety standards for pHRI. Then, the foundations of human-friendly robot design, including the development of lightweight and intrinsically flexible force/torque-controlled machines together with the required perception abilities for interaction are introduced. Subsequently, motion-planning techniques for human environments, including the domains of biomechanically safe, risk-metric-based, human-aware planning are covered. Finally, the rather recent problem of interaction planning is summarized, including the issues of collaborative action planning, the definition of the interaction planning problem, and an introduction to robot reflexes and reactive control architecture for pHRI.

The original version of this chapter was revised. The erratum to this chapter is available at DOI 10.1007/978-3-319-32552-1_81

69.1 Classification

Robotics is currently undergoing a fundamental paradigm shift, both in research and real-world applications. Classically, it was dominated for the last decades by possibly dangerous position-controlled rigid robots carrying out typical automation tasks, such as positioning and path tracking in various applications. Recently, a new generation of mechatronic robots has appeared on the landscape, including novel concepts in general robot design within the soft-robotics context. This trend brings us closer to the long-term goal of safe, seamless physical human–robot interaction (pHRI) in the real domestic and professional world (Fig. 69.1).

Recent advances in physical human–robot interaction have shown the potential and feasibility of robot systems for active and safe workspace sharing and collaboration with humans. The fundamental breakthrough was the human-centered design of robot mechanics and control (soft-robotics), which also induced the novel research stream of intrinsically elastic robots (series elastic actuators (SEA) or its generalization variable impedance actuators (VIA)). By considering the physical contact of the human and the robot in the design phase, possible injuries due to unintentional contacts can be considerably mitigated. Furthermore, taking into account the human's intention and preferences will enable the realization of human-friendly motions and interaction behavior. Some of the most advanced systems that were developed are now entering into industrial markets. These technologies serve both industrial and service-oriented domains. Possible future applications of these novel devices developed for close interaction with humans are depicted in Fig. 69.2. They range from industrial coworkers and mobile servants over robots in the professional service sector, assistive devices for physically challenged individuals, to service robots for the support of general household activities. All of these applications share the common requirement of close, safe, and dependable physical interaction between human and robot in a shared workspace. Therefore, such robots need to be carefully designed for human friendliness. That is, they have to be able to safely sense, reason, learn, and act in a partially unknown world inhabited by humans. In turn, this set of requirements necessitates the design of novel solutions in various theoretical and technological developments. In contrast to the classical modular view on robotics technology, and the role humans play in this, a fundamental paradigm shift in robot development has to be pursued. While encompassing safety issues based on biomechanical human injury analysis as well as on the kinesiologic biomechanics

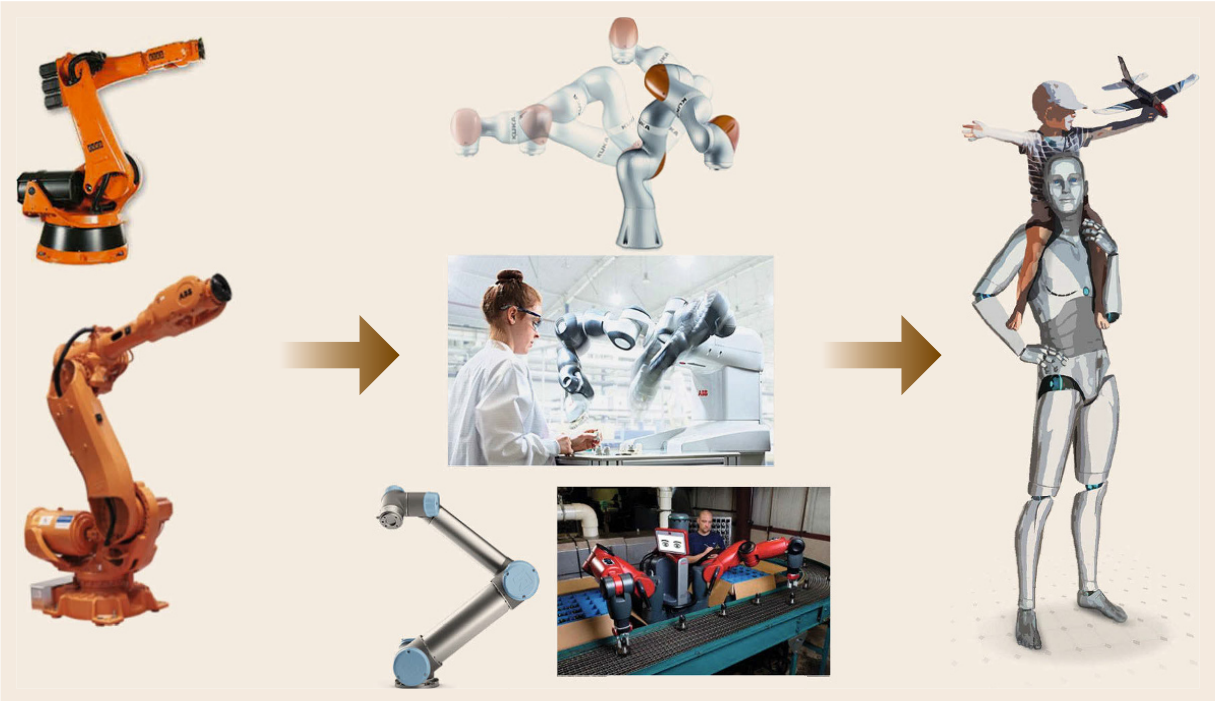

Fig. 69.1 The current paradigm shift in robotics induced by new target domains and robots toward the vision of close human–robot coexistence (courtesy of Keller und Knappich Augsburg (KUKA), Deutsches Zentrum für Luft- und Raumfahrt (DLR), ABB, Rethink Robotics)

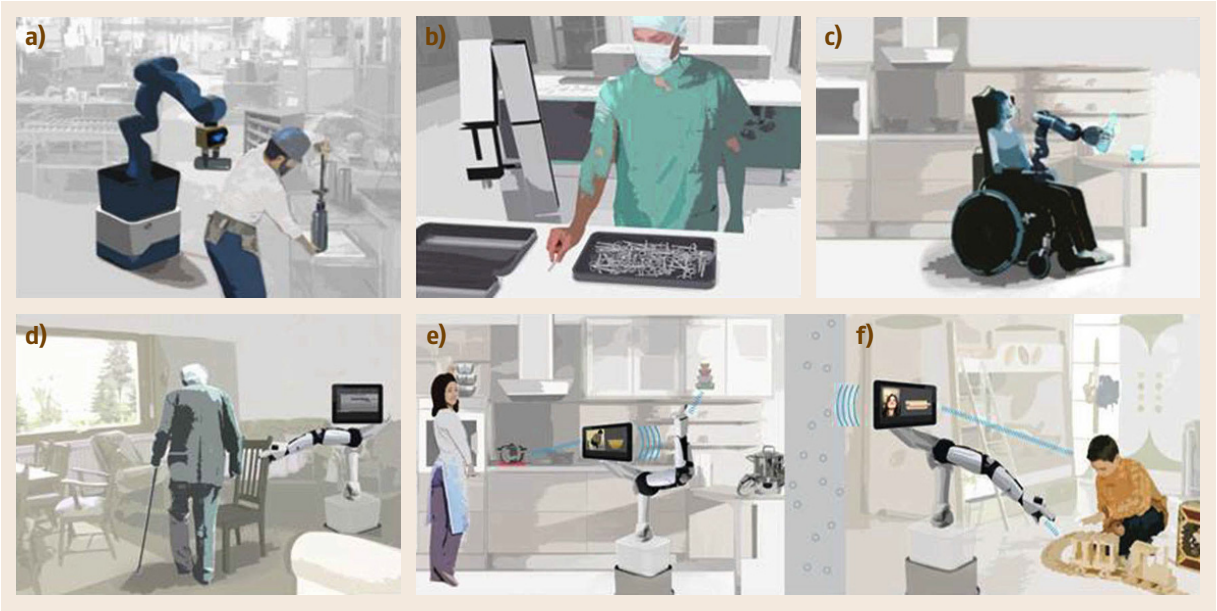

Fig.69.2a–f Application examples for pHRI, ranging from shop floor logistics and manipulation **(a,b)**, over professional service robots and assisitve devices for the disabled **(c,d)**, to service robots in domestic applications **(e,f)**

of human movements, human-friendly hardware design and interaction control strategies, learning, perceptive, and cognitive key components have to be developed and validated. These need to enable robots to track, understand, and predict human motions in real time in a weakly structured dynamic environment. Apart from developing the capabilities for interactive autonomy including self-improvement, human safety and physical interaction have to be embedded at the cognitive decisional level as well. This will enable the robots to react or physically interact with humans in a safe and autonomous way. Biomechanical knowledge, neuromechanical insights, and biologically motivated variable compliance actuators can be used to design manipulation/interaction systems of varying complexity close to human properties and performance. Further fundamental insights into novel designs of VIAs for an improved torque/mass ratio and energy efficiency with new control methods to exploit the stiffness and damping properties are required.

Planning and adapting motions and tasks of such complex systems in real-time require new concepts, including tight coupling of control, planning, and learning, which will lead to reactive behaviors capable of self-improvement. Moreover, self-explaining interaction and communication frameworks need to be developed to enhance the system usability and interpretability for humans. These should, for example, communicate whether a situation is safe or dangerous using not only verbal, but also nonverbal communication cues, such as gestures and emotional feedback. Finally, the dependability of all system components and algorithms is a major issue, the systematic treatment of which is of particular importance for subsequent industrial commercialization of the technology and also for the commercial domestic use of robots in everyday environments. Thus, the foreseeable breakthrough of the next generation of robotic systems in flexible automation in both small and medium enterprises (SMEs) and global market companies depends primarily on the pHRI development over the next years. Robotic assistance in manual processes that advantageously partner human and robot workers has an enormous unexplored potential to amplify productively in processes that previously could not be automated due to technological, cost, or efficiency reasons. Furthermore, very promising application domains of the technology are in the professional service sector (e.g., hospital support systems) and in the logistics domain (food logistics and quality inspection), which are so far to a large extent still purely manual work places. As the natural next step, systems capable of pHRI will enter the home sector as home assistants, elderly care assist, and assistive devices (VIDEO 607, VIDEO 614, VIDEO 618, VIDEO 623) for physically challenged people (VIDEO 618, VIDEO 619, VIDEO 620, VIDEO 621, VIDEO 622). First, rather basic tasks, such as fetch-and-carry or environment manipulation, will be solved followed by applications with increasing complexity.

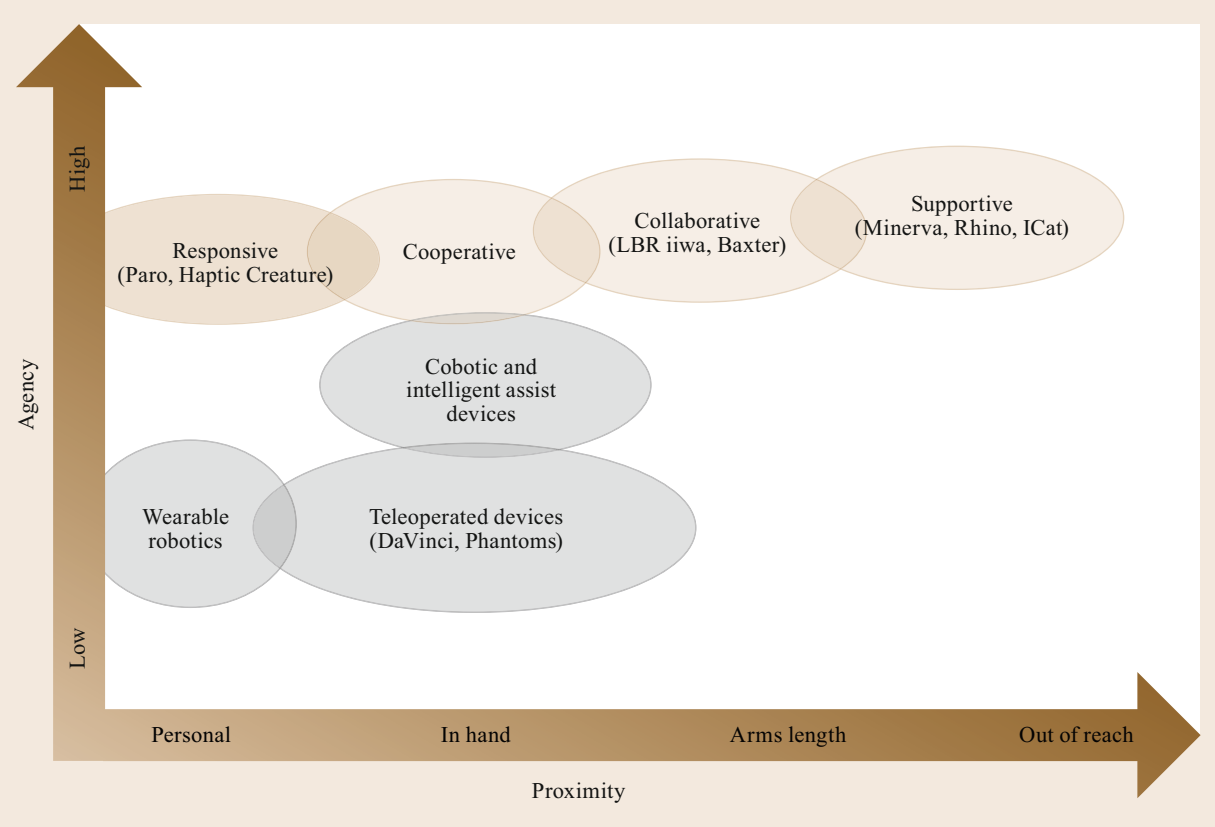

Fig. 69.3 Classification scheme for pHRI, by proximity of the interaction and agency (available autonomy) of the robot

69.1.1 Classification of Interaction

pHRI falls into the category of *proximate* interaction where humans and robots are colocated, as opposed to *remote* or teleoperated interaction (Chap. 43) [69.1]. Beyond proximity, the nature of the physical interaction can be understood in the context of the tasks and roles undertaken by the robot and human actors in a pHRI scenario. In all of these scenarios, a key feature is the available autonomy, or agency, of the robot partner for performing its portion of the task. This agency separates pHRI from Cobotic devices [69.2] and other passive robotic lift assists that require, by design, input from the operator.

Most work in pHRI can be generally classified across three broad categories of interaction: *supportive, collaborative, and cooperative*. Ordered in this way we note that these interactions are marked by increasing frequency and necessity of physical contact with the robot and level of proximity to the user (Fig. 69.3). Further categories include touch-based, personally responsive robots, for example, Paro [69.3] and the Haptic Creature [69.4], and wearable robots (Chap. 70).

In *supportive* interactions, we group interactions where the robot is not integral to the central performance of a task, but instead provides the human with the tools, materials, and information to optimize the human's task performance or objectives, for example, museum tour guide robots, shopping assistant robots for aiding seniors [69.5], and homecare robots (Chaps. 65 and 73). In this context, pHRI is typically concerned with safety, that is, preventing and mitigating the effect of unexpected contacts or collisions, and performing appropriate proxemic behavior. When required, physical interaction is infrequent and transitory in nature – typically limited to handoffs or other infrequent transactional exchanges. To support safety, as well as these limited physical interactions, well-structured human–robot communication (Chap. 71) is essential. For example, recent work [69.6–11] has demonstrated the importance of bi-lateral gesture cues in performing turn-taking, information sharing, close proximity activities, and precontact handover operations.

In *collaborative* interactions (VIDEO 609), the human and robot both work on the task, with the labor divided between the robot and human, each separately completing the parts of the task best suited to their

abilities, but more frequently interacting through turn-taking and part/tool passing [69.12, 13] (VIDEO 716), or haptically enabled mode switching where contact is used to switch the robot's interactive behavior [69.14] (VIDEO 717, VIDEO 632). In these scenarios, the human completes task elements requiring human dexterity or decision making, while the robot completes elements not well suited to direct human involvement, for example, repetitive or high-force applications, chemical deposition, or precision placement. In both supportive and collaborative interactions, physical space is often shared but planned physical interactions, although much more frequent, are still *transactional* in nature.

Cooperative interactions refer to the extension of cooperative manipulation (see also Chaps. 39 and 70) to include force interactions with humans. This type of interaction is differentiated from Cobots in that the robot operates as an independent agent, rather than a passive assist. That is, the human and the robot work in direct physical contact, or indirect contact through a common object, with continuous and cooperative shared control of the task. Cooperative interactions encompass tasks, such as cooperative lifting and carrying [69.15–17] (VIDEO 613, VIDEO 820), kinesthetic teaching [69.18] (VIDEO 627), coordinated material handling (e.g., managing long and flexible objects), and rehabilitation therapy (Chap. 64).

69.2 Human Safety

Providing safety in pHRI is a multifaceted challenge and requires an analysis on various levels of abstraction. pHRI aims at the coexistence of humans and robots in a common workspace and at extending their communication modes by physical means. This spatial proximity leads to a variety of *potential threats*, determined by the current state of the system of interest, which consists of the human(s), the robot(s), and their surrounding environment. Understanding the respective threats, in particular regarding potential human injury originating from physical robot–human contacts, and embedding the insights accordingly into safety standards/regulations is one of the major challenges of nowadays robotics (note that this chapter does not cover functional safety or robot dependability).

69.2.1 Human Injury in Robotics

Impact Scenarios

In order to quantify human injury that may occur in the context of pHRI, one needs to understand how mechanical contacts may cause injury in principle. Figure 69.4 depicts relevant robot–human impact scenarios. These may involve unconstrained impacts, clamping in the robot structure, constrained impacts, partially constrained impacts, and resulting secondary

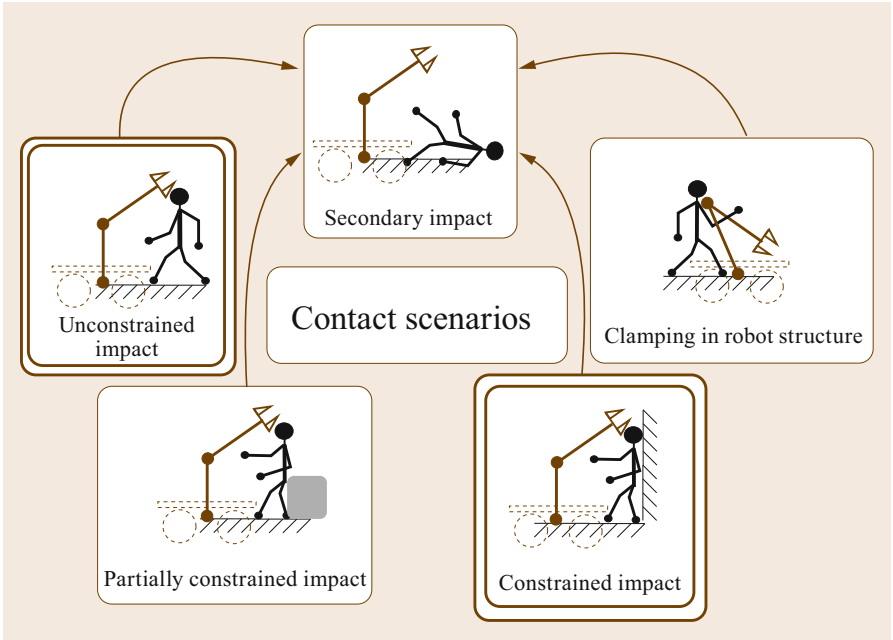

Fig. 69.4 Robot–human impact scenario classes. Unconstrained and constrained impacts are considered the two main scenarios

impacts [69.19]. Apart from such situational definitions, the most urgent question is how to quantify the human injury level that might occur due to a collision between human and robot. The understanding of human injury has been treated in the fields of injury biomechanics and forensics for several decades and the respective studies served for the early work on human injury in robotics. In fact, various injury measures from biomechanics and forensics were applied to human injury analysis in robotics [69.19–25]. An overview on the most important existing injury classification metrics and biomechanical injury measures can be found in [69.26] (VIDEO 608). The most important results from the biomechanics, forensics, and robotics literature are briefly reviewed now.

Overview Biomechanics Literature

In order to derive the injury characteristics of different body parts for direct collisions with an impactor, which is the most relevant case for robotics, countless experiments and publications have been produced over the last 50 years. The investigated impactors used in robotics and biomechanics experiments vary significantly in size and shape. However, from the test setups, one can identify and cluster principal geometric primitives. The main primitives and their parameters are depicted in Fig. 69.5. The z-axis of the coordinate frame associated with each primitive defines the direction of impact $\boldsymbol{u}$.

Numerous relevant impact experiments with cadavers, volunteers, crash test dummies, and biological tissue for the head, neck, and chest were generated (Tables 69.1–69.4). There for all selected experimental campaigns, the collision scenario, impacted body part, impact parameters according to Fig. 69.5, subject, and impact velocity are listed. For describing the collision scenario, we use the following abbreviations: D: dynamic, QS: quasi-static, U: unconstrained, C: constrained, PC: partially constrained. A collision experiment denoted by DU is, thus, dynamic unconstrained, while quasi-static constrained impacts are labeled QSC (Sect. 69.2.1, *Synopsis*). The respective impactor type and parameters are listed for comparison.

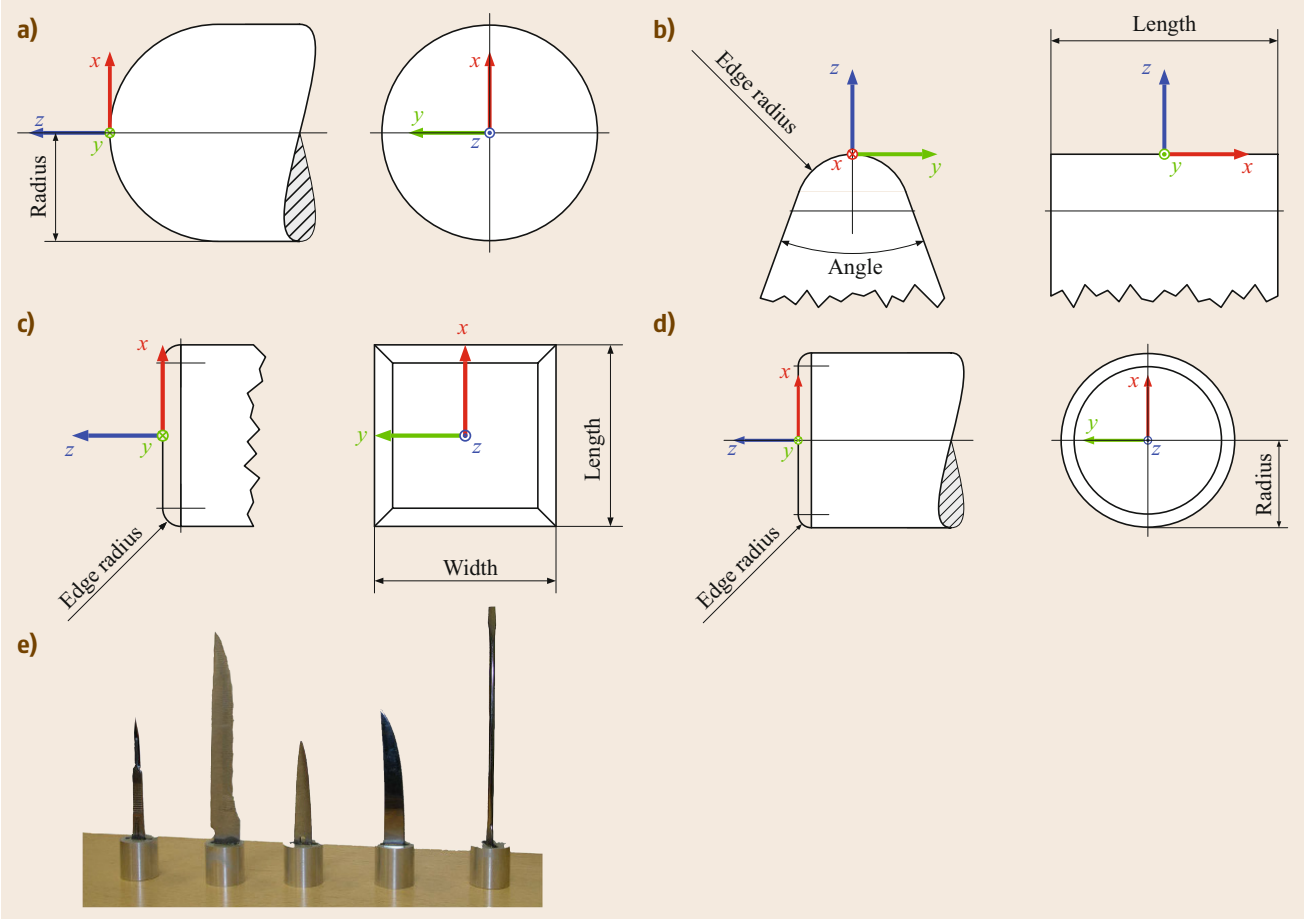

Fig.69.5a–e Typical impactor primitives with according parameters. **(a)** Sphere, **(b)** edge, **(c)** cuboid, **(d)** flat circular, **(e)** sharp tools

Table 69.1 Overview of selected impact experiments from biomechanics and robotics literature. Body part: Head

Impactor type	Impactor parameters	Collision case	Subject	Mass (kg)	Velocity (m/s)	References
Flat circular						
Maxilla, zygoma, frontal, temporo-parietal, mandible	14.3 mm radius	dynamic constrained (DC)	Cadaver	1.08–3.82	2.99–5.97	[69.27, 28]
Temporo-Parietal	12.7 mm radius	DC	Cadaver	10.6	2.7	[69.29]
Nose	14.3 mm radius	DC	Cadaver	3.2	1.56–3.16	[69.30]
Frontal	35 mm radius	DU	Cadaver	14.3	3.37–6.99	[69.31]
Edge						
Nose	12.5 mm radius	DU	Cadaver	32, 64	2.77–6.83	[69.32]
Maxilla, zygoma, frontal	10 mm radius	DC	Cadaver	14.5	2.4–4.2	[69.33]
Frontal	12.7 mm radius	dynamic partially constrained (DPC)	Cadaver	∞ (human falling on impactor)	2.23–3.14	[69.34]
Cuboid						
Temporo-parietal	50 mm length, 100 mm width	DC	Cadaver	12	4.3	[69.29]
Frontal	Size not specified, padded	DPC	Cadaver	5.31–5.97	3.56–9.6	[69.35]
Frontal	size not specified	DPC	Cadaver	∞ (human falling on impactor)	2.23–3.87	[69.34]
Sphere						
Frontal	120 mm radius	DU, QSC, DPC	Hybrid III dummy	4, 67, 1980	0.2–4.2	[69.36, 37]
Frontal	203.2, 76.2 mm radius	DPC	Cadaver	∞ (human falling on impactor)	2.87–3.5	[69.34]

Table 69.2 Overview of selected impact experiments from biomechanics and robotics literature. Body part: Torso

Impactor type	Impactor parameters	Collision case	Subject	Mass (kg)	Velocity (m/s)	References
Flat circular						
Thorax	76.2 mm radius, 12.77 mm edge radius	DU, DC	Cadaver	1.6–23.6	4.34–14.5	[69.38, 39]
Thorax	76 mm radius, rubber padded	DU	Volunteer	10	2.4–4.6	[69.40]
Thorax	76.2 mm radius, 12.77 mm edge radius	DU	Cadaver	19.27	4.0–10.6	[69.41]
Abdomen	12.7 mm radius	DU	Cadaver	32, 64	4.9–13.0	[69.42]
Sphere						
Thorax	120 mm radius	DU, QSC	Hybrid III dummy	4, 67, 1980	0.2–4.2	[69.36, 37]
Abdomen	5, 12.5 mm radius	DC	Pig tissue	2–10	0.5–4.0	[69.25]
Edge						
Abdomen	45° angle, 200 mm length, 0.2 mm edge radius	DC	Pig tissue	2–10	0.5–4.0	[69.25]

Table 69.3 Overview of selected impact experiments from biomechanics and robotics literature. Body part: Upper extremities

Impactor type	Impactor parameters	Collision case	Subject	Mass (kg)	Velocity (m/s)	References
Edge						
Forearm	12.5 mm radius, angle 0°	DC	Cadaver	9.48	3.63	[69.43]
Forearm	size not specified	DC	Cadaver	9.75	2.44, 4.23	[69.44]
Shoulder, upper arm, forearm	5 mm edge radius, 30° angle	DC	Volunteer	4.16, 8.65	0.45–1.25	[69.45]
Flat circular						
Forearm, hand	size not specified	QSC	Cadaver	∞ (velocity control)	25 mm/min	[69.46]

Table 69.4 Overview of selected impact experiments from biomechanics and robotics literature. Body part: Lower extremities

Impactor type	Impactor parameters	Collision case	Subject	Mass (kg)	Velocity (m/s)	References
Sharp	Fig. 69.5	DC	Pig tissue, volunteer	4	0.16–0.8	[69.24]

Next, some essential characteristics of human–robot impacts are elaborated for a more general understanding of the underlying dynamics.

Robot–Human Impacts

Let us assume that of a serial chain rigid robot consisting of n joints, there is at most a single link involved in a collision. Let

$$\dot{\boldsymbol{x}}_{\mathrm{c}} = \begin{pmatrix} \boldsymbol{v}_{\mathrm{c}} \\ \boldsymbol{\omega}_{\mathrm{c}} \end{pmatrix} = \begin{pmatrix} \mathbf{J}_{\mathrm{c,lin}}(\boldsymbol{q}) \\ \mathbf{J}_{\mathrm{c,ang}}(\boldsymbol{q}) \end{pmatrix} \dot{\boldsymbol{q}} = \mathbf{J}_{\mathrm{c}}(\boldsymbol{q})\dot{\boldsymbol{q}} \in \mathbb{R}^6 \quad (69.1)$$

be the stacked (screw) vector of linear velocity at the contact point and the angular velocity of the associated robot link, with an associated (geometric) contact Jacobian $\mathbf{J}_{\mathrm{c}}(\boldsymbol{q})$ that is a function of the joint angle $\boldsymbol{q}$. Accordingly, the Cartesian collision wrench is denoted by

$$\boldsymbol{\mathcal{F}}_{\mathrm{ext}} = \begin{pmatrix} \boldsymbol{f}_{\mathrm{ext}} \\ \boldsymbol{m}_{\mathrm{ext}} \end{pmatrix} \in \mathbb{R}^6 \,. \quad (69.2)$$

Robot Collision Modeling. When such a collision occurs, the robot dynamics becomes

$$\mathbf{M}(\boldsymbol{q})\ddot{\boldsymbol{q}} + \mathbf{C}(\boldsymbol{q}, \dot{\boldsymbol{q}})\dot{\boldsymbol{q}} + \boldsymbol{g}(\boldsymbol{q}) + \boldsymbol{\tau}_{\mathrm{F}} = \boldsymbol{\tau} + \boldsymbol{\tau}_{\mathrm{ext}} \,, \quad (69.3)$$

where $\mathbf{M}(\boldsymbol{q}) \in \mathbb{R}^{n\times n}$ is the symmetric and positive definite joint space inertia matrix, $\mathbf{C}(\boldsymbol{q}, \dot{\boldsymbol{q}})\dot{\boldsymbol{q}} \in \mathbb{R}^n$ is the centripetal and Coriolis vector, and $\boldsymbol{g}(\boldsymbol{q}) \in \mathbb{R}^n$ is the gravity vector; $\boldsymbol{\tau} \in \mathbb{R}^n$ is the motor torque, and $\boldsymbol{\tau}_{\mathrm{F}} \in \mathbb{R}^n$ is the dissipative friction torque; $\boldsymbol{\tau}_{\mathrm{ext}} \in \mathbb{R}^n$ is the typically unknown external joint torque given by

$$\boldsymbol{\tau}_{\mathrm{ext}} = \mathbf{J}_{\mathrm{c}}^{\mathrm{T}}(\boldsymbol{q})\, \boldsymbol{\mathcal{F}}_{\mathrm{ext}} \,. \quad (69.4)$$

The effective mass $m_{\boldsymbol{u}}$ of a robot acting in the instantaneous collision direction $\boldsymbol{u}$, which has to be consistent to $\mathbf{J}_{\mathrm{c}}(\boldsymbol{q})$, can be deduced from $\mathbf{M}(\boldsymbol{q})$ via the Cartesian kinetic energy matrix $\boldsymbol{\Lambda}(\boldsymbol{q})$. This is defined as

$$\boldsymbol{\Lambda}(\boldsymbol{q}) = \left[\mathbf{J}_{\mathrm{c}}(\boldsymbol{q})\mathbf{M}(\boldsymbol{q})^{-1}\mathbf{J}_{\mathrm{c}}(\boldsymbol{q})^{\mathrm{T}}\right]^{-1} \,, \quad (69.5)$$

where the inverse of $\boldsymbol{\Lambda}(\boldsymbol{q})$ is based on the decomposition of the kinetic energy matrix

$$\boldsymbol{\Lambda}(\boldsymbol{q})^{-1} = \begin{bmatrix} \boldsymbol{\Lambda}_{v}(\boldsymbol{q})^{-1} & \overline{\boldsymbol{\Lambda}}_{v\omega}(\boldsymbol{q}) \\ \overline{\boldsymbol{\Lambda}}_{v\omega}(\boldsymbol{q})^{\mathrm{T}} & \boldsymbol{\Lambda}_{\omega}(\boldsymbol{q})^{-1} \end{bmatrix} , \quad (69.6)$$

with $\overline{\boldsymbol{\Lambda}}_{v\omega}(\boldsymbol{q}) = \mathbf{J}_{\mathrm{c,lin}}(\boldsymbol{q})\mathbf{M}(\boldsymbol{q})^{-1}\mathbf{J}_{\mathrm{c,ang}}(\boldsymbol{q})^{\mathrm{T}}$. Finally, $m_{\boldsymbol{u}}$ is found to be

$$m_{\boldsymbol{u}} = [\boldsymbol{u}^{\mathrm{T}}\boldsymbol{\Lambda}_{v}(\boldsymbol{q})^{-1}\boldsymbol{u}]^{-1} \,. \quad (69.7)$$

It should be noted that the Jacobian has to be the *center-of-mass-Jacobian*. Otherwise, the entire inverse of the Cartesian inertia tensor has to be used, and not just its translational component block. More details can be found in [69.47]. We assume the local impact curvature in the $\boldsymbol{u}$-direction to be denoted by $c_{\boldsymbol{u}}$.

Characteristic Robot–Human Impact Force Profile. A physical collision between robot and human is typically characterized by a distinct force profile that is composed by two consecutive phases (note that for unconstrained soft-tissue collisions these two phases can simplify into a single *Phase I* impact) (Fig. 69.6):

1. Phase I is characterized by a very short impact, governed by the robot- and human-reflected dynamics.
2. Phase II is characterized by a quasistatic contact event. Without clamping, this is a pushing force, whereas if the human is clamped it is a crushing force.

Phase I can be treated from a pure impact physics, almost open-loop point of view, that is, it is determined by the reflected inertia, velocity, and impact curvature $c_{\boldsymbol{u}}$ of the robot together with the characteristics of the respective body part that is being struck. The maximum contact force is denoted F_{I}.

Phase II, on the other hand, has to be further subdivided into either *clamping* or *no clamping* incident. In the case of no clamping, the maximum force is F_{IIA}, whereas for clamping, the maximum force is F_{IIB}. In particular, *Phase II* is highly robot control and design dependent and is especially important in the case of clamping:

- *Phase IIA*: *No clamping*. Typically, for free impacts at robot velocities $> 0.3\,\mathrm{m/s}$, F_{IIA} is significantly smaller than F_{I}. Otherwise, F_{I} is smaller than F_{IIA} and is governed by the robot actuator torques (active quasistatic pushing) and the reaction of the human body that is mainly governed by its reflected impedance.
- *Phase IIB*: *Clamping*. In the case of clamping, the final maximum force F_{IIB} is limited by the maximum motor torques $\boldsymbol{\tau}_{\max}$ of the robot via $\boldsymbol{\mathcal{F}}_{\mathrm{ext}} = \mathbf{J}_{\mathrm{c}}^{\mathrm{T\#}}\boldsymbol{\tau}_{\max}$, where $\mathbf{J}_{\mathrm{c}}^{\mathrm{T\#}}$ is the contact Jacobian pseudoinverse. If the robot is powerful enough to generate active contact forces that penetrate or break human tissue/structure, the contact force is, of course,

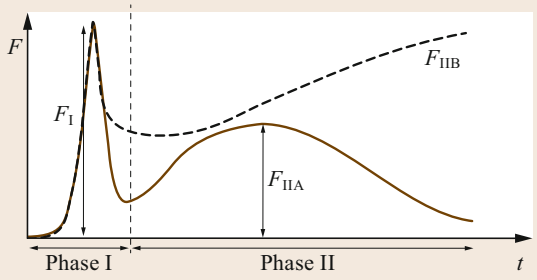

Fig. 69.6 Typical robot–human collision force profiles

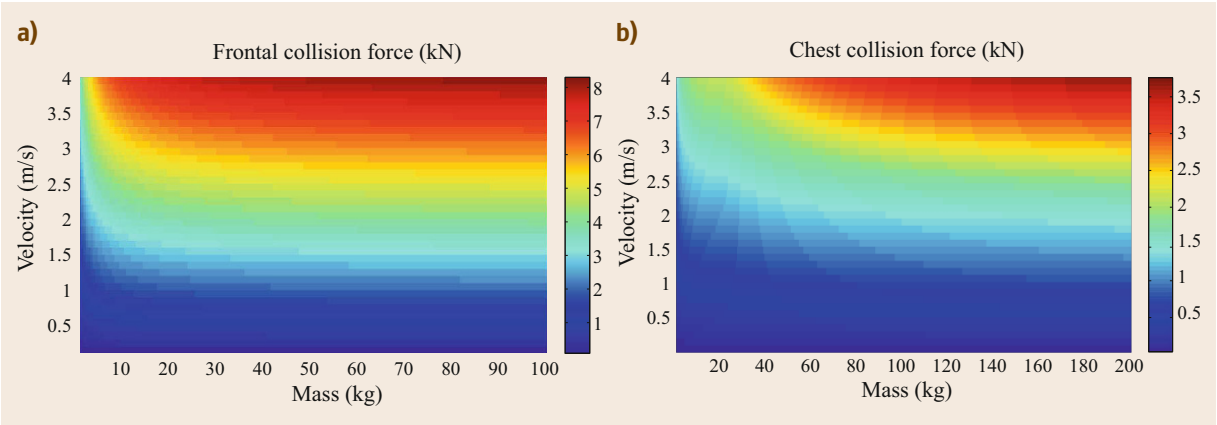

Fig.69.7a,b Mass–velocity dependency for **(a)** human head and **(b)** chest contact force. A mass–spring-mass model is used for collisions against the head, where the head mass M_H is 4.5 kg and the approximate contact stiffness of the frontal bone $K_H = 1000\,\mathrm{N/mm}$ (after [69.33]). For the chest, the model proposed in [69.48] is used

limited by the human maximum tissue resistance. Please note that singularities need careful treatment, which, however, goes beyond the scope of the chapter.

Next, the influence of robot mass and velocity for the unconstrained impact are described. This analysis is particularly important to understand Phase I.

Influence of Robot Mass and Velocity. Assume a simple mass–spring-mass model for the impact between human and robot. M_H is the reflected inertia of the human. K_H is the contact stiffness, which is in the case of a rigid robot mainly the effective stiffness of the human contact area. $\dot{x}_{re}^0$ is the relative impact velocity between the robot and human. Solving the corresponding differential equation leads to the maximum contact force

$$\mathcal{F}_{ext}^{max} = \sqrt{\frac{m_u M_H}{m_u + M_H}}\sqrt{K_H}\dot{x}_{re}^0 \,. \tag{69.8}$$

Assume a simplifying decoupling of the head from the torso, which holds for the short duration of the impact. For the post-impact phase, neck stiffness and body inertia have to be considered, which complicates the analysis considerably. The dependency of frontal bone contact force on the robot mass and velocity is depicted in Fig. 69.7a. It can be observed that collision force (which is a well-known bone fracture indicator) generally increases with velocity. For increasing mass, however, a saturation effect takes place. After a certain robot mass has been reached ($m_u \approx 20\,\mathrm{kg}$ in Fig. 69.7), additional weight has only negligible influence on collision force. This inertial saturation effect can also be observed for other impact locations, such as contacts with the chest (Fig. 69.7b).

If the robot mass is significantly larger than the human head mass, that is, $m_u \gg M_H$, (69.8) reduces to

$$\mathcal{F}_{ext}^{max}(m_u \gg M_H) = \sqrt{K_H M_H}\dot{x}_{re}^0 \,. \tag{69.9}$$

This shows that for a robot with significantly larger reflected inertia than the human head, only the contact stiffness, the impact velocity, and the mass of the human head are relevant but not the robot mass.

The behavior of human tissue during collisions is complex. Consequently, surrogates cannot reveal the entire diversity. Accordingly, the conduction of human voluntary experiments is necessary to fully understand human injury and pain dynamics in robotics.

Human–Robot Impact Voluntary Testing

The following experimental test was the first systematic analysis in this direction. The voluntary experiments were conducted with a healthy young adult in the year 2011. The collision experiments were performed with the KUKA/DLR lightweight robot (LWR) and the following approaches to injury and pain analysis were carried out: *injury severity analysis according to AO* (Arbeitsgemeinschaft für Ostheosynthesefragen), *biomechanical analysis*, *pain*, and *imaging methods*. The setup and experiment steps are depicted in Fig. 69.8. The robotic system allows to conduct controlled robot–human collisions in order to analyze input parameters and their effect on output parameters, such as pain and injury. Measured impact characteristics and quantities included impact force, impact area, tissue displacement, tissue stiffness, stress, impact velocity, kinetic energy, and energy density. The reflected inertia

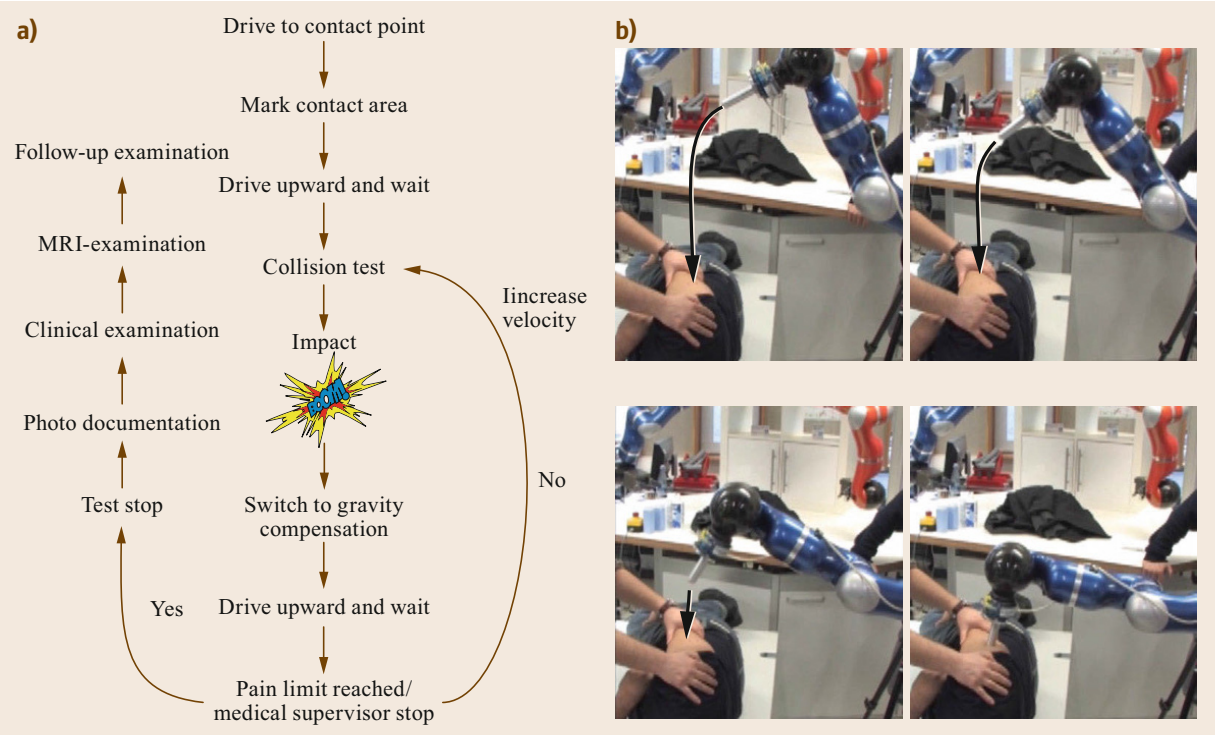

Fig. 69.8 **(a)** Flow chart depicting the basic experimental steps. **(b)** Collision trajectory with subject

was kept constant at $m_u = 3.75\,\text{kg}$ for every test. The used impactor for the resulting Table 69.5 was a sphere with a radius of 12.5 mm.

The injury was defined using the AO-classification [69.49] directly after each test series. Each impact series was carried out at the same location on the human body at increasing impact velocity until the participant initiated a controlled system stop during the experiment. The impact areas were then imaged with a magnetic resonance imaging (MRI) after a time interval of about 4–5 h. The remaining tissue did not show any pathological signs. Compared to an equivalent drop test in [69.25] with abdominal pig tissue (large sphere, 4.2 kg, 2.5 m/s), the voluntary experiments provide similar results in terms of injury severity. The maximum velocity of 2.55 m/s is at the border of inducing a contusion. Where there were no marks immediately after impact, a mild contusion formed at day 1. For the pain tolerance at a visual analog scale (VAS) of 6/10, an impact force of $F = 272.2\,\text{N}$ was measured. The energy density appears to have the most significant correlation to pain.

Synopsis

An overview of the potential injury threats depending on the current state of the robot and the human, a classification of these mechanisms, governing factors of the particular process and possible injuries are depicted in Fig. 69.9. Physical contact can be divided into two fundamental subclasses: quasi-static and dynamic loading. Fundamental differences in injury severity and mechanisms are observed as well if a human is (partially) constrained or not, leading to the second subdivision. For the quasi-static case, it is differentiated between near-singular and nonsingular clamping as already outlined. The last differentiation separates injuries caused by blunt contact from the ones induced by tools or sharp surface elements.

Each class of injury is characterized by possible injuries (PI), worst-case factors (WCFs), and their worst-case range (WCR). WCFs are the main contributors to the worst case, such as maximum joint torque, the distance to singularity or the robot speed. The worst-case range indicates the maximum possible injury depending on the worst-case factors. In addition to the classification of injury mechanisms for each such class, suggestions for injury measures (IMs) are given as well. They are specific injury measures which are appropriate, useful for the classification and measurement of injury potentially occurring during the physical human–robot interaction. Please note that the list of injury measures is not necessarily complete, but these ones are certainly suitable to be applied to a more granular robotics injury analysis. This does not mean that criteria, such as the well-known head injury criterion (HIC), do not provide general insights; they are just not

Table 69.5 Impact data for the lateral surface of the right upper arm

Impact	Max. impact force (N)	Impact area (mm^2)	Displacement (m)	Tissue stiffness (N/m)	Stress σ (N/mm^2)	Impact velocity (m/s)	Kinetic energy (J)	Energy density (J/mm^2)	AO	VAS
1	9.5	966	0.03	316.7	0.001	0.2	0.08	0.0001	IC1MT1NV1	0
2	19	966	0.037	513.5	0.002	0.44	0.36	0.0007	IC1MT1NV1	0
3	38.1	966	0.044	865.9	0.039	0.65	0.80	0.0016	IC1MT1NV1	0
4	59.6	966	0.055	1083.6	0.062	0.88	1.45	0.003	IC1MT1NV1	0
5	81.4	966	0.058	1403.4	0.084	1.11	2.31	0.005	IC1MT1NV1	1
6	103.5	966	0.060	1725	0.107	1.34	3.37	0.007	IC1MT1NV1	1.5
7	128.1	966	0.064	2001.6	0.133	1.55	4.50	0.009	IC1MT1NV1	2
8	154.1	966	0.069	2233.3	0.16	1.76	5.81	0.012	IC1MT1NV1	3
9	186.4	966	0.069	2701.4	0.193	2.03	7.73	0.016	IC1MT1NV1	3
10	224.5	966	0.069	3253.6	0.253	2.24	9.41	0.019	IC1MT1NV1	4
11	272.2	966	0.077	3535.1	0.282	2.55	12.2	0.025	IC1MT1NV1	6

necessarily optimal to understand injury on a more differentiated lower-injury scale.

For example ① in Fig. 69.9 represents blunt clamping in the near-singular configuration (Fig. 69.9). Even for low-inertia robots, this situation could become dangerous and is, therefore, a possible serious threat with almost any robot on a fixed base within a (partially) confined workspace. Possible injuries are fractures and secondary injuries, for example, caused by penetrating bone structures or an injured neck if the trunk is clamped but the head is free. This would mean that the robot pushes the head further, while the trunk remains in its position. Another possible threat is shearing off a locally clamped human along an edge. Appropriate indices are, for example, the contact force and the compression criterion (CC) [69.50]. ③ in Fig. 69.9 represents the clamped blunt impact in nonsingular configuration. The injury potential is defined by the maximum actuation torque $\boldsymbol{\tau}_{\max}$ and can range from no injury to severe injury or even death for high-inertia (and torque) robots. The robot stiffness does not contribute to the worst case since a robot without collision detection would simply increase the motor torque to follow the desired trajectory. Therefore, robot stiffness only contributes to the detection mechanism by enlarging the detection time. Also, the contact force and CC are well suited to predict occurring injury. ⑧ in Fig. 69.9 denotes the unconstrained impact which was the first injury mechanism investigated in the robotics literature. This process is governed by the impact velocity and (up to a saturation value) by the robot mass. As shown in [69.22], even a robot of arbitrary mass cannot severely injure a human head by means of impact-related criteria from the automobile industry like the head injury criterion (HIC). However, fractures, for example, of facial bones are likely to occur but not all would be classified as a serious injury. Laceration by means of crushes and gashes are worth evaluating, especially with respect to service robotics. The contact force and CC are well-suited severity criteria for this class. In order to evaluate lacerations the energy density has to be considered.

The preceding overview is intended as a worst-case analysis for the described contact cases. The next step is to ask which actions can be taken against each particular threat [69.19]. At this point, however, it shall be noted that instead of quantifying injury in terms of a measurable injury criterion, injury evaluation by a medical expert, for example, via the AO-classification can always be applied and would presumably result in a more exhaustive and precise judgement.

69.2.2 Safety Standards for Human–Robot Interaction

Robotics standardization made significant progress to establish the underlying regulations for co-working cells in the real world. Safety for industrial robots is addressed in a variety of general standards [69.51–53]. The most important industrial robotics standards is the International Organization for Standardization (ISO) 10218. It was established in the recognition of the particular hazards that industrial robots and industrial robot systems may pose. The machinery concerned and the extent to which hazards, hazardous situations, and events are covered are indicated in the scope of ISO 10218. In recognition of the variable nature of hazards with different uses of industrial robots, ISO 10218 is divided into two parts. It provides a detailed analysis of mechanical hazards, such as impacts, crushing, shearing, entanglement, drawing-in or tapping, cutting or severing, and contact of persons with live parts (direct contact) [69.54]. In particular, the introduction of collaborative robots has been a ma-

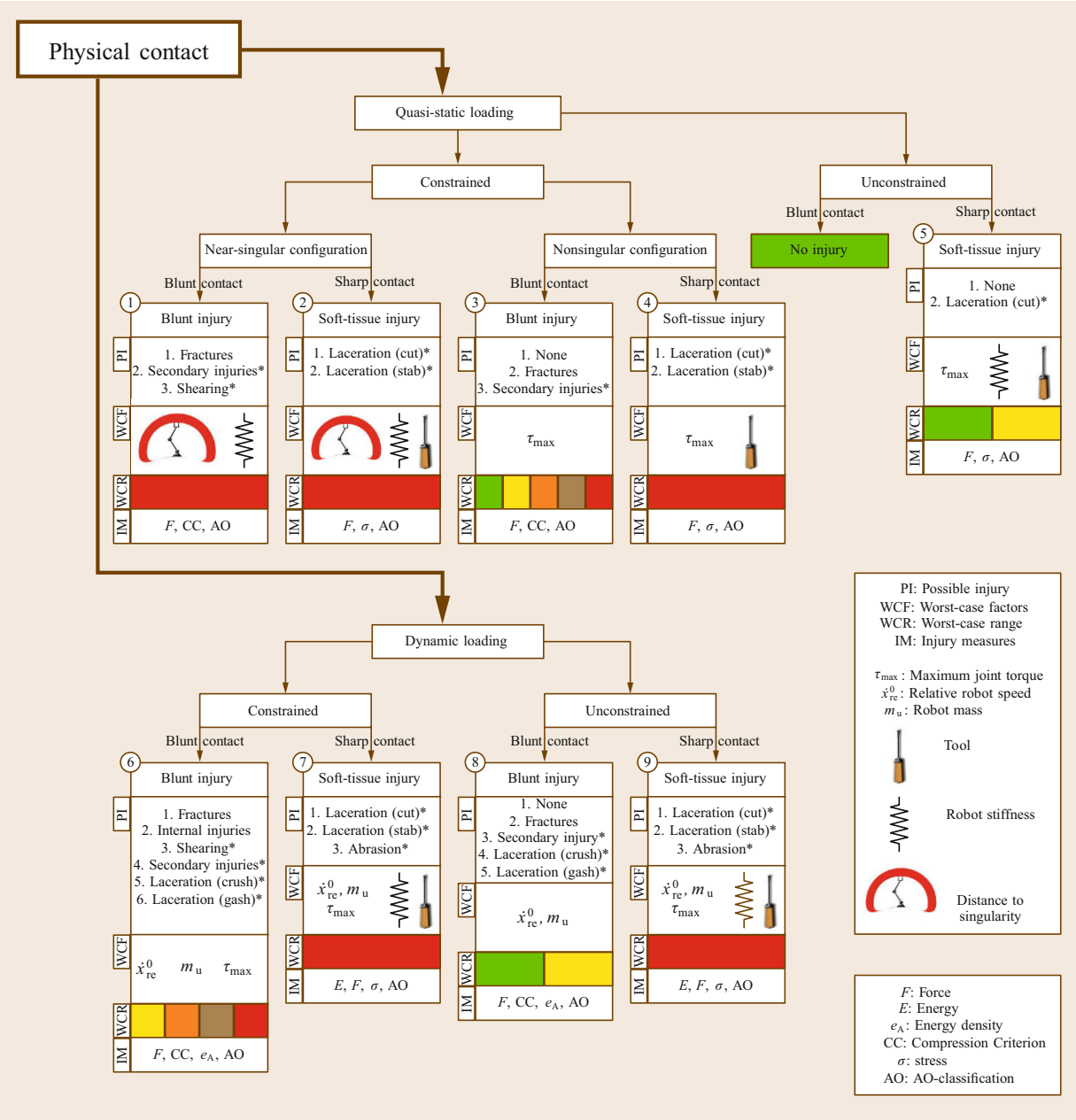

Fig. 69.9 Safety tree showing possible injury (PI), major worst-case factors (WCF) and the possible worst-case range (WCR). * indicates still ongoing topics of research. Additionally, relevant injury criteria are given for the head, chest, and soft-tissue injuries

jor acknowledgment to the advances made in robotics research in pHRI over the last decade. The recent updates to ISO 10218 (safety requirements for industrial robots) led to the development of the new technical specification (TS) 15066. It is regarded as a complementary information that concretizes the content of ISO 10218. Generally, ISO/TS 15066 provides guidance for collaborative robot operation where a robot and a person share the same workspace. It considers collaborative modes and requirements, such as minimum separation distances, safety-rated monitored stops, speed and separation monitoring, and power and force limiting. In collaborative operations, the integrity of the safety-related control system is of major importance, particularly when process parameters, such as speed and force, are being controlled. A comprehensive risk assessment is required to assess not only the robot system itself, but also the environment in which it is

placed, that is, in the workplace. A key process in the elimination of hazards and reduction of risks is the design of the collaborative robot system and the associated cell layout. Various considerations about the access and clearance of the collaborative workspace are provided. During the design of a robotic system, the maximum space and the restrictions of the collaborative robot system have to be considered. Furthermore, the need for clearances around obstacles and the accessibility for operators should influence the design. The intended contact(s) between parts of the robot system and an operator plays a major role toward a possibly intrinsically safe design. In order to identify the risks resulting from the collaborative action, an appropriate set of collision incidents that can occur during the collaborative work activities and foreseeable misuse has to be determined. This has to include affected body regions and the involved collision areas of the robot. The limit values that may not be exceeded during the collision incident depend on the affected body regions. The geometry of the involved areas of the robot and the biomechanical properties of the affected body regions influence the forces occurring during the collision incident. Therefore, the ISO/TS 15066 describes injury severity criteria that consist of maximum allowable limit values on individual body regions. These limit values are established to prevent the occurrence of skin/tissue penetrations that are accompanied by bleeding wounds, fractures, or other skeletal damage [69.55].

In addition to the industrial standardization efforts in the pHRI domain, the ISO 13482 [69.56] is the first nonindustrial robot safety standard that allows/regulates close pHRI. This international standard specifies requirements and guidelines for the inherent safe design, protective measures, and information for the use of so called *personal care robots*. It focuses on three types of personal care robots (mobile servant robots, physical assistant robots, and person carrier robots). These robots typically perform tasks to improve the quality of life of intended users irrespective of age or capability. The standard describes hazards associated with the use of these robots and provides requirements to eliminate or reduce the risks associated with these hazards to an acceptable level. Significant hazards are presented and this standard describes how they are to be dealt with for each personal care robot type. Robotic devices used in personal care applications are also covered by this standard and are to be treated as personal care robot.

69.3 Human-Friendly Robot Design

Designing robots for interaction has become a challenging subdomain in pHRI, leading to novel devices that have one thing in common: active and/or passive compliance together with lightweight design being the central design paradigms. A number of research-focused robots have been designed specifically for pHRI. The most important design guidelines, representatives, and modeling basics are outlined in this section. Apart from robots that are designed to act as general purpose co-workers, large robot assists with balanced, inertia reducing, cable-driven gantry systems can be used to create large payload robots that may be operated next to human workers [69.57].

69.3.1 Lightweight Design

In the process of making robots inherently suitable for close physical interaction with humans or only partially known environments, a design paradigm shift moving away from heavy, stiff, and rigid designs toward lightweight and highly integrated mechatronics designs has taken place. Low inertia and high (active) compliance have become desirable features, as has the use of redundant sensing principles on the proprioceptive level (position, velocity, and torque).

General Characteristics

Generally, two major design approaches for lightweight robots have proven successful over the last years [69.58], namely the *mechatronics approach* and the *tendon-based approach*, respectively. Their commonalities are as listed:

- *Lightweight structures*: Lightweight, high-strength metals, or composite materials for the robot links. Moreover, the design of the entire system (controllers, power supply) is optimized for weight reduction to enable mobility.
- *Low power consumption*: This is mainly achieved by small moving inertias and accordingly designed motors.

Typically, *mechatronic robots* integrate electronics into the joint structure for allowing highly modular units. Such a design enables the assembly of different kinematics with increasing complexity, while keeping the respective joint philosophy. In terms of actuation,

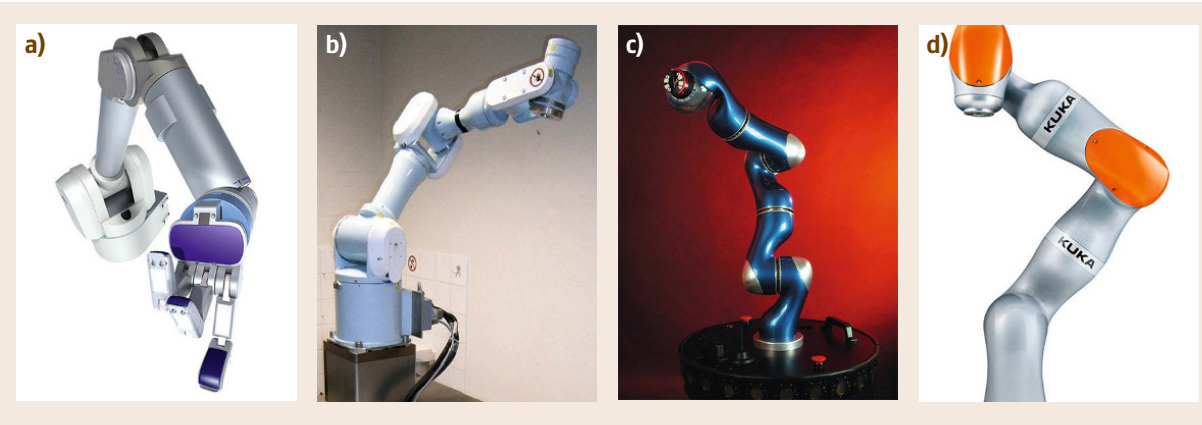

Fig. 69.10 (a) Barrett arm (after [69.59]), (b) Mitsubishi PA10 arm, (c) DLR lightweight robot III (after [69.60]), (d) KUKA LBR iiwa (after [69.61]) (courtesy of Barret Technology Inc., DLR, KUKA)

the combination of high power/torque motors with high transmission ratio gears is usually applied. From the proprioceptive sensing side, these systems are typically equipped with additional sensors, such as joint torque, force, and current sensing in addition to basic motor side position and current sensing only (Sect. 69.3.3).

Tendon-based robots have three major characteristics. First, they are typically equipped with remote direct drives. This reduces the overall weight of moving parts for a fixed base manipulator as the actuators are located in the robot base. For placing the actuators remotely from the base, cable-pulley systems are usually applied. Finally, low reduction ratios are used for keeping the system backdrivable. In turn, larger motors have to be selected, which adds additional total weight.

Another interesting class of compliant actuators is of note that implements compliance quite differently. They use rheological fluids such that they can alter their characteristic properties under the influence of either a magnetic or an electric field. A clutch between link and motor is operated in such a way that the output torque can be controlled. These actuators were also motivated and discussed from a human-safety perspective in [69.62].

Lightweight Robotic Systems

The most prominent robots that fall into the category of lightweight robots are depicted in Figure 69.10. The *Barrett arm* is a classic example of a *tendon-based design*, where the actuators are placed in the manipulator base and the joints are backdrivable due to the low reduction ratio. The *Mitsubishi PA10* arm was a commercially available lightweight redundant arm, with a weight of 38 kg and a payload of 10 kg. The fully torque-controlled *KUKA LBR iiwa* is based on the DLR lightweight robot technology [69.61]. Its third generation DLR LWR-III weighs 13.5 kg and is able to handle loads up to 15 kg, so an approximate unitary payload-to-weight ratio is achieved. The robot is equipped with joint torque sensors in each joint and has redundant position measurement (on motor and link side) [69.63].

Apart from single-arm robots as described above, various lightweight designs were also successfully integrated into research and commercial humanoid systems

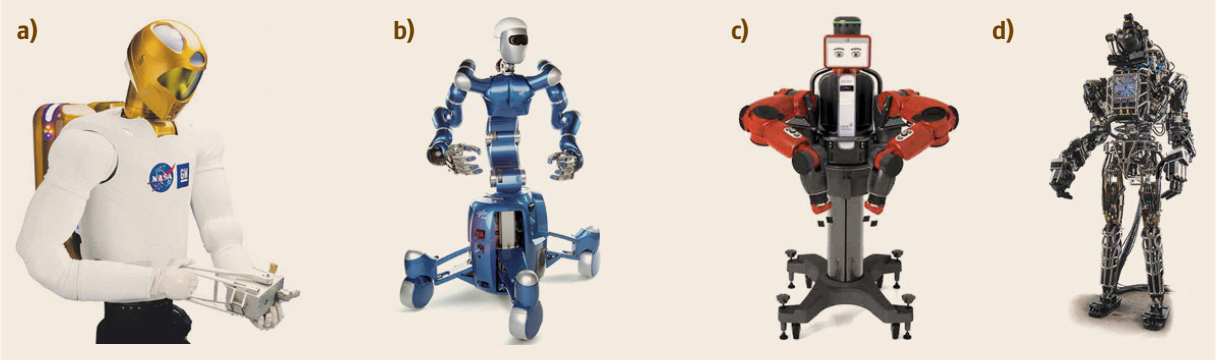

Fig. 69.11 (a) NASA *Robonaut 2*, (b) DLR *Rollin' Justin*, (c) Rethink Robotics *Baxter* and (d) Boston Dynamics *Atlas* (courtesy of NASA, DLR, Rethink Robotics Inc., Boston Dynamics)

(Fig. 69.11). The NASA (National Aeronautics and Space Administration) *Robonaut 2* [69.64], equipped with SEA, was originally designed for teleoperation and exploration in space [69.65]. The fully torque-controlled humanoid robot TORO [69.66], based on the DLR lightweight robot technology, has its origins in the upper body bimanual system *Justin* [69.67] (VIDEO 626). Rethink Robotics *Baxter* is a commercial two-arm upper body system for pick and place tasks that is equipped with SEA for torque measurement purposes. The hydraulically actuated humanoid, *Atlas* from Boston Dynamics, is one of the systems that entered the *DARPA (Defense Advanced Research Projects Agency) Robotics Challenge*.

Modeling Lightweight Robots

For a robot with n viscoelastic joints, the so-called reduced model of *Spong* [69.68] has become the standard way of modeling lightweight robots. When including also the presence of joint torques due to contact forces (on the link dynamics), we shall consider the following dynamic model of robots with viscoelastic joints:

$$\mathbf{M}(\boldsymbol{q})\ddot{\boldsymbol{q}} + \mathbf{C}(\boldsymbol{q},\dot{\boldsymbol{q}})\dot{\boldsymbol{q}} + \boldsymbol{g}(\boldsymbol{q}) = \boldsymbol{\tau}_{\mathrm{J}} + \boldsymbol{\tau}_{\mathrm{ext}}\,, \tag{69.10}$$

$$\mathbf{B}\ddot{\boldsymbol{\theta}} + \boldsymbol{\tau}_{\mathrm{J}} = \boldsymbol{\tau}\,. \tag{69.11}$$

The generalized coordinates are doubled since there will be a dynamic displacement $\boldsymbol{\delta} = \boldsymbol{\theta} - \boldsymbol{q}$ between the motor positions $\boldsymbol{\theta} \in \mathbb{R}^n$, as reflected through the gear ratios, and the link positions $\boldsymbol{q}$. The matrix $\mathbf{B} = \mathrm{diag}(B_i) \in \mathbb{R}^{n\times n}$ is the diagonal, positive definite motor inertia matrix. We define the *elastic joint torque* transmitted through the joints and coupling (69.10) and (69.11)

$$\boldsymbol{\tau}_{\mathrm{J}} = \mathbf{K}_{\mathrm{J}}(\boldsymbol{\theta} - \boldsymbol{q}) + \mathbf{D}_{\mathrm{J}}(\dot{\boldsymbol{\theta}} - \dot{\boldsymbol{q}})\,, \tag{69.12}$$

where $\mathbf{K}_{\mathrm{J}} = \mathrm{diag}(K_{\mathrm{J},i}) \in \mathbb{R}^{n\times n}$ is the diagonal, positive definite joint stiffness matrix, and $\mathbf{D}_{\mathrm{J}} = \mathrm{diag}(D_{\mathrm{J},i}) \in \mathbb{R}^{n\times n}$ is the diagonal, positive semidefinite joint damping matrix. The quantity $\boldsymbol{\tau}_{\mathrm{J}}$ in (69.12) is also the output of joint torque-sensing devices, when available. In many practical cases, the mechanical design of the transmission/reduction elements is such that one can neglect the joint damping, that is, $\mathbf{D}_{\mathrm{J}} \simeq \mathbf{0}$. Joint elasticity has long been addressed for lightweight robot systems, however, more as an undesired consequence that the control has to handle [69.69]. This requires advanced control techniques in order to obtain accurate, performant motion. For a complete overview on the properties of robots with joint elasticity effects, please refer to Chap. 11.

69.3.2 Intrinsically Flexible Design

Recently, the class of intrinsically flexible actuators and robots have become increasingly popular. Inspired by the flexible properties in biological muscles, compliant joints are designed with the aim of imitating human or animal motions during various tasks. The main idea of intrinsically flexible actuation is to come closer to human capabilities in terms of speed and shock absorption. This is not realizable with todays rigid industrial robots, when assuming approximately the same torque range or weight as humans have. By storing and releasing energy in the joints, one aims for improvement in tasks, such as running or throwing [69.70–73] where humans still clearly outperform robots. In Chap. 21 and [69.74], a more in depth review of intrinsically flexible actuation is presented. In this chapter, we review only the relevant insights for placing the technology in the pHRI context.

General Characteristics

Roughly speaking, intrinsically flexible actuators can be divided into two categories:

- Actuators with fixed mechanical impedance, where the effective joint impedance is altered via active control. The most well-known example is the series elastic actuator (SEA) [69.75], whose acronym became a generic term for this class of actuators.
- Actuators where the impedance can be adjusted by altering mechanical joint properties, such as stiffness and damping. There exist various categories like variable stiffness actuators (VSAs) that allow stiffness changes or variable impedance ac-

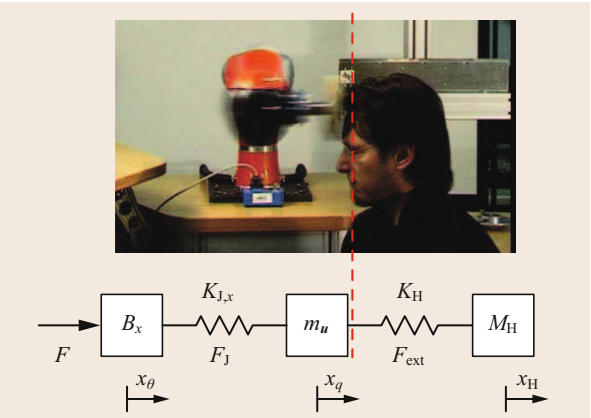

Fig. 69.12 Human–robot collision in operational space, which is defined by the reflected flexible dynamics of the robot and the local contact stiffness/mass properties of the human head

tuators (VIAs) that enable more general impedance changes, including damping adjustment.

The original motivation for introducing VSA and VIA, for example, in [69.20], was to make robots safer during unforeseen collisions due to dynamic decoupling of the motor and link-side inertia from each other. This effect reduces the collision danger by alleviating the impacting robot inertia. In [69.20], it is, for example, shown that HIC could be reduced by introducing elasticity in the joint. This idea was generalized and systematically analyzed in [69.76, 77], and is summarized here.

In order to simplify the human robot collision analysis basic models in operational space coordinates were used for this analysis (Fig. 69.12). For this, operational space coordinates and reflected inertias/stiffnesses along an arbitrary instantaneous impact direction $\boldsymbol{u}$ are considered [69.47]. The masses $M_{\mathrm{H}}, m_{\boldsymbol{u}}, B_x \in \mathbb{R}^+$ are the reflected human, link, and motor mass. $K_{\mathrm{H}}, K_{\mathrm{J},x} \in \mathbb{R}^+$ are the reflected (human) contact stiffness and joint/structural elasticity. The projected human, motor, and link impact position are denoted by x_{H}, x_θ, and $x_q \in \mathbb{R}$, respectively. $x_\theta = p_{\boldsymbol{u}}(T(\boldsymbol{\theta}))$ and $x_q = p_{\boldsymbol{u}}(T(\boldsymbol{q}))$ are defined via the respective forward kinematics maps projected in the $\boldsymbol{u}$-direction.

As pointed out in [69.20], a robot with quite low reflected link inertia $m_{\boldsymbol{u}} = 0.1\,\mathrm{kg}$ is able to reduce the impact forces significantly if a contact stiffness of $K_{\mathrm{H}} = 5\,\mathrm{kN/m}$ is assumed. Similar to the work in [69.21], it was shown that a decrease in joint stiffness can significantly reduce the impact characteristics and, thus, is a powerful countermeasure against large contact forces. In [69.78], it was deduced that for the case of a 2-DOF (degree of freedom) planar intrinsically compliant robot, already slightly touching a rigid wall with its second link, the compliant mechanism can limit the maximum static force/torque effectively if the motor torque is slowly increased. It is, of course, unquestionable that joint elasticity decouples the motor from the link. However, as was indicated in [69.22], a reduction in joint stiffness cannot reduce the impact characteristics during very rigid, fast, and blunt crash-test dummy impacts for a lightweight system, such as the LWR-III (which is basically an SEAs type robot from a modeling perspective). This was proven by measuring the decoupling of motor and link inertia via the integrated joint torque sensors and the additionally recorded external contact force.

Figure 69.13 depicts the experimental evidence for a collision at 1 m/s between a DLR LWR-III and a stationary unconstrained Hybrid III dummy (HIII) head on the frontal area [69.22]. The contact force f_{ext} was measured with a high-speed force sensor $f_{\mathrm{ext,fs}}$ and for consistency check with a triaxial accelerometer $f_{\mathrm{ext,as}}$. As one can see, the simulation and experimental signals show very good consistency. Clearly, the projected elastic joint force f_{J} reacts delayed to the collision, thus proving the desired decoupling property already for such an intrinsically very stiff robot. For the impact simulation, a reflected stiffness of $6.72 \times 10^4\,\mathrm{N/m}$ is chosen, which represents a realistic joint stiffness and structural elasticity value. The reflected motor inertia is $B_x = 13\,\mathrm{kg}$ and the reflected link side inertia $m_{\boldsymbol{u}} = 2\,\mathrm{kg}$. The dummy head mass is $M_{\mathrm{H}} = 4.5\,\mathrm{kg}$ and the contact stiffness is $K_{\mathrm{H}} = 3.2 \times 10^5\,\mathrm{N/m}$.

This result showed that already the compliances of the built in gear and the joint torque sensor is sufficient to decouple the motor from the link, making it entirely unnecessary to further reduce joint stiffness for the given robot for this purpose. There are two main aspects, which have to be considered to fully understand this result. On the one hand, the contact stiffness of the crash-test dummy used is significantly larger than the reflected elasticity of the DLR LWR-III; however, it is also realistic for the human frontal area [69.27]. Furthermore, the reflected motor and link inertia for the DLR LWR-III are the same order of magnitude as for the human head mass. This is quite reasonable for a full-scale lightweight robot arm.

Two further benefits of inherent compliance are as follows. First, the robot itself is able to resemble compliant behavior without the inherent need for high-performance force/torque feedback. Please note that it is not possible to display arbitrary Cartesian stiffness behavior for a robot with diagonal stiffness matrix only [69.80]. Second, the joint elasticity acts in combination with the link inertia as a mechanical low-

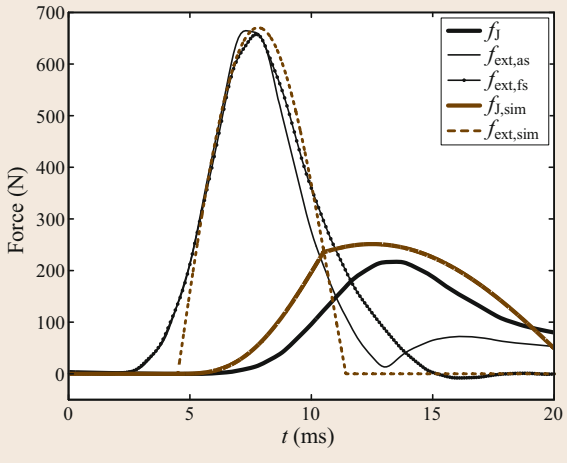

Fig. 69.13 Impact experiment and simulation of a LWR-III with a Hybrid III Dummy. The experimental contact force is measured for consistency check with a high-speed acceleration (as) and force sensor (fs) simultaneously

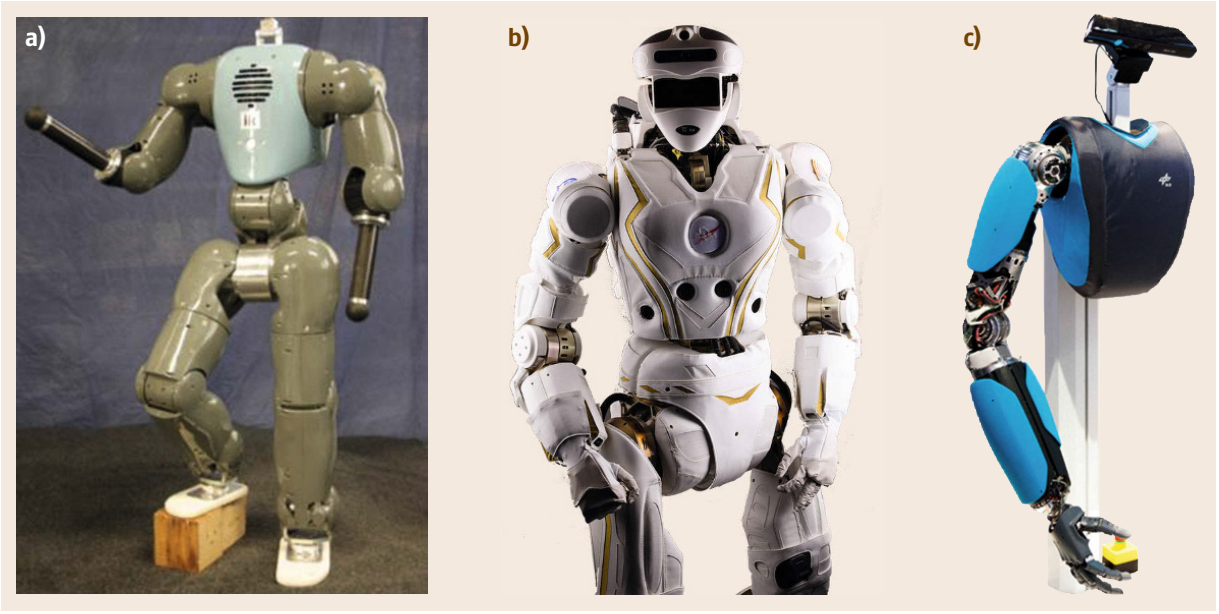

Fig.69.14a–c Passively flexible anthropomorphic robots: compliant humanoid platform (COMAN, **(a)**) from IIT (after [69.79]), Valkyrie **(b)** from NASA, and hand arm system (HASY, **(c)**) from DLR (courtesy of IIT, DARPA, DLR)

pass filter, thus protecting the drive train from impact shocks; that is, it makes the system inherently more robust [69.72, 81].

Another interesting use of elasticities in the drive train of a manipulator relates to the fact that it can serve as a storage mechanism for potential energy, and be used to increase a robot's link speed beyond the maximum motor velocity [69.71, 72, 81–83]. This ability strongly influences the safety of intrinsically elastic systems, as a robot's impact speed determines its inherent collision danger to a large extent. However, we refer to [69.76] for further details on this matter, where the effect of a robot's elastic speed increase on potential danger in terms of HIC is derived.

Intrinsically Flexible Robotic Systems

Figure 69.14 shows some of the most prominent recent anthropomorphic/humanoid devices that employ passively compliant actuators. The COMAN system of IIT (VIDEO 624) is a full-scale SEA robot, as is NASA's Valkyrie. Both system's ability to measure torques results from the ability to flex around their joint axes and then relate this elastic deflection to the joint torque. The DLR hand-arm system [69.73] is fully equipped with VSA in every joint, while having approximately human size, strength, and dexterity.

Modeling Passively Flexible Robots

From a formal modeling point of view, lightweight robots and robots with fixed mechanical impedance are very similar. The main difference lies in the respective torque sensor measurement principle. The joint elasticity in lightweight robots is rather high and allows only for small deflections between the motor and link position. The stiffness in compliant actuators, however, is intentional and typically at least an order of magnitude lower, thus enabling significantly larger deflections. Consider the elastic joint model (69.10) and (69.11) from Sect. 69.3.1, which under certain mild conditions also holds for intrinsically elastic robots. The main difference is that for lightweight robots, $K_{\mathrm{J},i}$ is large compared to *SEA-like* systems. For many VSA systems, the transmitted torque can be expressed as

$$\boldsymbol{\tau}_{\mathrm{J}} = \boldsymbol{f}(\boldsymbol{\delta}, \boldsymbol{\sigma}) \,, \tag{69.13}$$

where $\boldsymbol{\sigma}$ denotes a stiffness adjustment control input (typically the position of a second motor). The torque–displacement curve $\boldsymbol{f}(\boldsymbol{\delta}, \boldsymbol{\sigma})$ may exhibit different characteristics, such as being strictly increasing $\partial \boldsymbol{f}(\boldsymbol{\delta}, \boldsymbol{\sigma})/\partial \boldsymbol{\delta} > \mathbf{0}$ and convex $\partial^2 \boldsymbol{f}(\boldsymbol{\delta}, \boldsymbol{\sigma})/\partial \boldsymbol{\delta}^2 > \mathbf{0}$. More details on implementations can be found in [69.74].

69.3.3 Perception for Interaction

The recent advances in pHRI benefit greatly from previous achievements in contact and noncontact sensors and sensing techniques. In the current chapter, we shortly review the essential sensing techniques that had strong

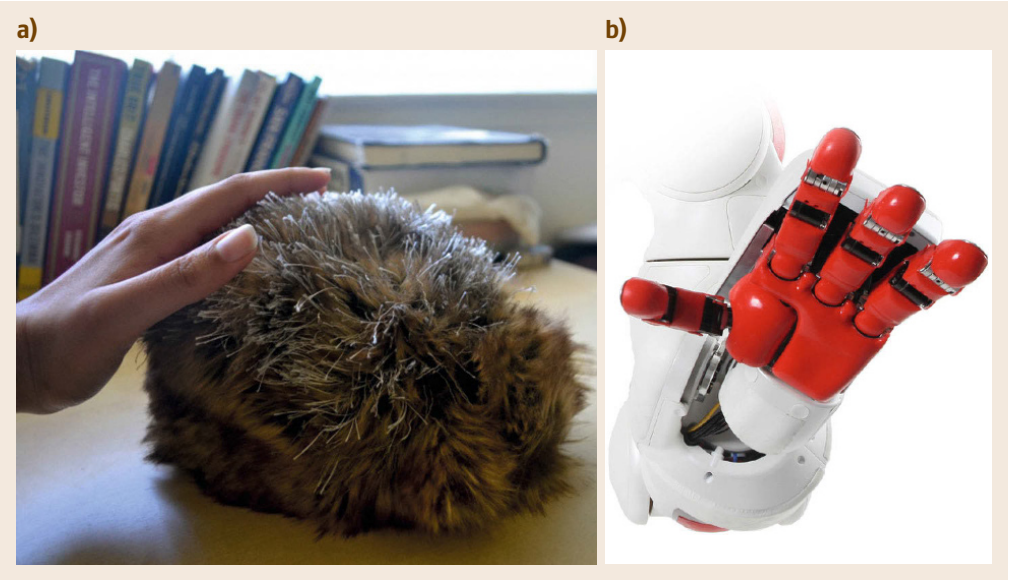

Fig. 69.15 **(a)** Furry robot *skin* utilizing piezo-resistive fabric and conductive sensors provides a low cost design concept with high tactile gesture recognitions rates (after [69.84]). **(b)** The hand of TWENDY-ONE with integrated distributed pressure sensors (courtesy of Karon MacLean, UBC, Shigeki Sugano Lab., Waseda University)

impact on pHRI and focus on the underlying main concepts. Chapters 28 and 32 give a full view and can be consulted for further details.

69.3.4 Proprioceptive Force/ Torque Sensing

Many robot arms have the option to include a six-axis force/torque sensor at the wrist, enabling not only force control-based manipulation, but also symbolic haptic interaction [69.85, 86], possibly also based on joint torque sensing. More recently, torque sensors have been integrated into the joints of commercial robots, for example, into the KUKA LWR [69.87]. This allows for contact sensing along the entire robot structure with measurements of contact magnitude, direction, and knowledge of which link was contacted [69.88].

Essentially, two major sensing principles for joint torque measurement exist: either by directly measuring the torque which is typically done via strain gauges, or by measuring it implicitly via the deflections $\boldsymbol{\delta}$ between link and motor position. For this, it is assumed that $\boldsymbol{\delta}$ directly relates to torque typically by a constant multiplier, the joint stiffness $K_{\mathrm{J},i}$. For the latter, both link- and motor-side position sensors need to be mounted. The first works that aimed at developing and minimizing torque-sensing devices can be found in [69.89–91]. The torque-sensing principle has also a strong relation to the design classification in Sect. 69.3.

69.3.5 Tactile Perception

Several tactile skins have been developed over the years such as, for example, [69.92–95]. In the latter work, for example, the human skin served as a design metaphor. Therein, a solution of the goal conflict between the desired high sensitivity and the required mechanical robustness is in the focus. Furthermore, beyond providing the required sensory capability, the mechanical deformation and damping properties necessary for the operation of the robotic system are considered as well. Using whole-arm tactile sensing across the manipulator surface explicitly allows the sensing of multiple contacts; for example, in [69.96], the authors operate a robot in a cluttered environment in order to successfully reach a goal that is occluded by obstacles using a model predictive controller. Other recent examples of localized sensors include touch pads placed at key points on the robot [69.97], and force-sensitive resistors distributed over the robot [69.98]. The latter example is used in a novel haptic robot designed to both read and display emotion mediated through cues sensed primarily through physical interaction. These methods have the advantage of using reliable and fairly precise sensors, but are capable of measuring contact only at discrete locations. For more extensive contact sensing, several researchers have developed various types of robot skin; that is a distributed sensor network that covers extensive areas and measures diverse qualities of contact events, including location, magnitude, orientation, and temperature. Hard robot skins or shells have been used

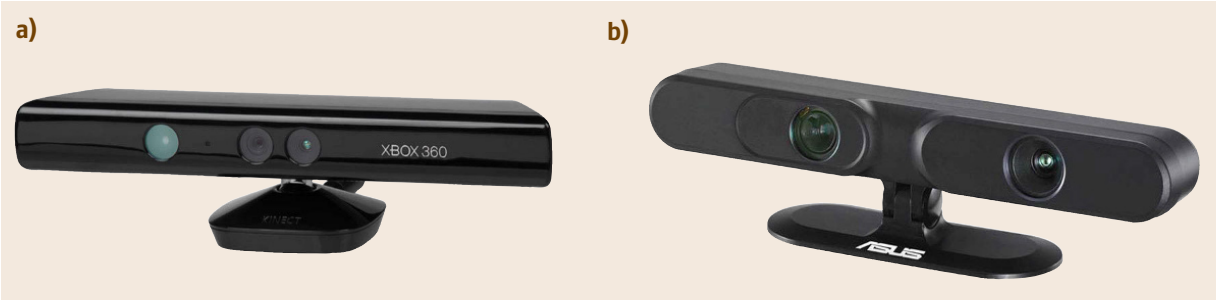

Fig. 69.16 Low cost 3-D-RGB-D cameras: (a) Microsoft Kinect (Wikipedia Commons), (b) Asus Xtion (courtesy Asus)

to detect collisions [69.99], while soft robot skins that can conform to different robot shapes have been used for more complex, often social or affective, human–robot interaction, for example, [69.100]. While robot skin can add significant sensing capability to robots, it may also add to the complexity and cost, and thus compromises the robustness of the robot. However, recently a furry *creature* skin (Fig. 69.15) was created [69.84] using a combination of low-resolution piezo-resistive fabric, and conductive fur sensors to create a low-cost robot covering with 90% interaction gesture (stroking, patting, poking, hitting) recognition rates when trained on an individual and 68–80% recognition rates when trained on groups (VIDEO 615). A detailed review of tactile sensing technology for human–robot interaction can be found in [69.101]. Other examples can be found in Chap 28.

69.3.6 Visual Perception

Visual (noncontact) sensing is very important for preparing for pHRI. Tracking and planning for the location of a human partner and predicting, for example, the motion of the partner's hand is an important precursor to a successful handover operations [69.12]. While well-known marker-based systems, such as Vicon and Optotrak systems, provide very high resolution tracking systems, they are impractical for day-to-day use. The development of low-cost 3-D-RGB-D (three-dimensional red green blue depth) cameras (Fig. 69.16) permits the 3-D tracking of full body models in large and partially occluded spaces, with ongoing improvements toward robustness in body pose tracking and for tracking of hand gestures [69.102, 103].

69.4 Control for Physical Interaction

For soft and safe pHRI, the question arises how to gently handle physical contact in robotics from a control point of view. As impedance control [69.104] became the most popular interaction control paradigm in the pHRI world, this particular scheme will be one focus of this section. Its generalization to multipriority impedance control laws allows the realization of sophisticated robot compliance with multiple objectives via active control. A major advantage of impedance control is that discontinuities like contact–noncontact do not create stability problems as they occur, for example, with hybrid force control [69.105]. Its extension to impedance and feed-forward learning and adaptation, for which the first works can be found in [69.106, 107], is discussed after introducing the concept of multipriority impedance control. Apart from nominal interaction control, a robot sharing its workspace with humans and physically interacting with its environment should be able to quickly detect collisions and safely react to them. In the absence of external sensing, relative motions between robot and environment/human are unpredictable and unexpected collisions may occur at any location along the robot arm. The state-of-the-art schemes for collision detection and reflex reaction are introduced. Finally, the last part of the section deals with the shared manipulation problem, one of the standard application examples of pHRI.

69.4.1 Interaction Control

Originally developed for robust and compliant object manipulation, impedance and the related admittance control (VIDEO 610) form a paradigm to treat robotic systems from an energetic point of view such that motion and force can be controlled in a unified manner. They offer the advantage over hybrid force-motion controllers to provide a framework independent from kinematic work space constraints. These control types popularized by [69.104] are also especially advantageous in terms of uncertainties and disturbances in

unknown environments due to their inherently robust nature [69.108]. The terms impedance and admittance, are derived from electrical system theory where they describe the relationship between voltage and current as input/output pairs. To generalize impedance and admittance such pairs can be defined domain-independently as effort and flow variables. For robotics, the mechanical analogies, that is, mechanical impedance and admittance are of particular interest.

More details on the conceptual basics of impedance and the dual admittance control can, for example, be found in [69.109, 110]. Furthermore, Chap. 9 gives a more thorough basis on force control strategies in general and impedance control in particular.

The mostly used version of impedance control is to impose a second-order dynamics of a mass–spring–damper system (so-called target impedance [69.104]) on the closed-loop equations. Typically, the control objective is expressed in operational space coordinates $\boldsymbol{x}$ as

$$\mathbf{M}_x\ddot{\tilde{\boldsymbol{x}}} + \mathbf{D}_x\dot{\tilde{\boldsymbol{x}}} + \mathbf{K}_x\tilde{\boldsymbol{x}} = \boldsymbol{\mathcal{F}}_{\text{ext}} \,, \tag{69.14}$$

where $\tilde{\boldsymbol{x}} := \boldsymbol{x} - \boldsymbol{x}_{\text{d}}$ is the position error and $\boldsymbol{x}_{\text{d}}$ is called equilibrium position. $\mathbf{M}_x$ denotes the desired inertia, while $\mathbf{D}_x$ and $\mathbf{K}_x$ are the according closed-loop damping and stiffness matrices in operational space. $\boldsymbol{\mathcal{F}}_{\text{ext}}$ denotes the external wrench acting at the end-effector of the robot. Assuming rigid body dynamics, the control law to obtain the aforementioned behavior is

$$\begin{aligned}\boldsymbol{\tau}_{\text{C}*} = {} & \boldsymbol{g}(\boldsymbol{q}) + \mathbf{J}(\boldsymbol{q})^{\text{T}}[\boldsymbol{\Lambda}(\boldsymbol{q})\ddot{\boldsymbol{x}}_{\text{d}} + \boldsymbol{\mu}(\dot{\boldsymbol{x}}, \boldsymbol{x})] \\ & - \mathbf{J}(\boldsymbol{q})^{\text{T}}\left[\boldsymbol{\Lambda}(\boldsymbol{q})\mathbf{M}_x^{-1}(\mathbf{K}_x\tilde{\boldsymbol{x}} + \mathbf{D}_x\dot{\tilde{\boldsymbol{x}}})\right] \\ & + \mathbf{J}(\boldsymbol{q})^{\text{T}}\left[\boldsymbol{\Lambda}(\boldsymbol{q})\mathbf{M}_x^{-1} - \mathbf{I}\right]\boldsymbol{\mathcal{F}}_{\text{ext}} \,. \end{aligned} \tag{69.15}$$

In order to fully implement this scheme, a wrist force torque sensor is necessary for the inertia shaping part. In [69.111], a modified impedance controller was designed that uses angle/axis representations for the rotational components of the operational space. For its derivation, energy contributions with physical interpretation are considered and the end-effector orientation displacement representation is chosen to be in terms of a unit quaternion to avoid singularities.

For redundant robots, it is typically desired to also control the nullspace behavior in order to embed other control objectives $\boldsymbol{\tau}_{N,i}$ into a stacked hierarchy of tasks (Chaps. 17 and 36). For the case of a single nullspace controller $\boldsymbol{\tau}_N$, this torque has to be projected via the nullspace projector matrix $\mathbf{N}(\boldsymbol{q})$ into the nullspace of the task, leading to the overall control law

$$\boldsymbol{\tau}_{\text{C}} = \boldsymbol{\tau}_{\text{C}*} + \mathbf{N}(\boldsymbol{q})^{\text{T}}\boldsymbol{\tau}_N \,. \tag{69.16}$$

The nullspace projection matrix can be chosen in different ways. The simplest case is $\mathbf{N}(\boldsymbol{q}) = \mathbf{I} - \mathbf{J}(\boldsymbol{q})^{\#}\mathbf{J}(\boldsymbol{q})$, where $\mathbf{J}(\boldsymbol{q})^{\#}$ denotes the Moore–Penrose pseudoinverse. Alternatively, one may chose the *dynamically consistent* generalized pseudoinverse

$$\mathbf{J}(\boldsymbol{q})^{\#} = \mathbf{M}(\boldsymbol{q})^{-1}\mathbf{J}(\boldsymbol{q})^{\text{T}}\boldsymbol{\Lambda}(\boldsymbol{q}) \,. \tag{69.17}$$

In particular, in the pHRI domain, a multitude of different subtasks $\boldsymbol{\tau}_{N,i}$ are meaningful to be executed simultaneously. These may, for example, involve:

- Safety (collision anticipation and avoidance, self-collision avoidance, ...)
- Physical constraints (joint limits, geometric task constraints)
- Task execution (tracking control, ...)
- Posture primitives (in particular for humanoids).

To realize consistent behaviors, task hierarchies are constructed such that certain tasks are prioritized over others [69.112]. In [69.113], a hierarchy is realized by null space projection techniques, which also prevents discontinuities concerning unilateral constraints by smoothing out transitions.

Extensions to the basic schemes for flexible joint dynamics [69.114–116] and for the SEA case [69.117] were developed as well. Furthermore, Cartesian impedance control has been applied to grasping and multiple-arm robotic systems in [69.118]. For a more in depth treatment of multipriority impedance control, please also refer to Chap. 67.

69.4.2 Learning and Adaptation

Close physical interaction between human and robot is a complex evolving process with high uncertainty and is hard to be modeled explicitly. Therefore, several learning and adaptation approaches were proposed to enhance a robot's capability and account for the inherently present uncertainty and unpredictability. In this sense, the extension of impedance control toward adaptive controllers that are able to learn and/or adapt the controller's impedance and feed forward torques is a challenging and rather recent research problem. Obviously, also the learning of the desired trajectories, for example, in terms of motion patterns became an important problem in this context. Generally, also collaborative tasks (Sect. 69.4.4) require learning either the impedance properties and/or certain trajectories such that the robot gains the ability to adapt its behavior to the human counterpart, or even guides it to guarantee successful collaboration. An important aspect of learning physical interactions is how to choose the right task coordinates and (meta-)parameters. This is essential to reformulate the otherwise high-dimensional problem spaces in a tractable form.

Since impedance control has already shown to be a valuable technique in cluttered and complex manipulation tasks, recent research focuses on the adaption of the impedance characteristics to further improve the robot capabilities during interaction. Iterative learning control techniques belong to the first methods that have been investigated to tackle difficult manipulation problems [69.119, 120]. However, they do not only require the exact same repetitive motion of the manipulator, but also to account for unforeseen changes in the environment due to force inconsistencies which are particularly present in pHRI. Other early approaches include, for example, the use of neural networks in impedance control to counteract disturbances and environmental uncertainties [69.121]. An approach to adapt force, trajectory, and impedance simultaneously has been presented in [69.122] as a biomimetic controller. It is constructed based on studies in neuroscience that show that humans adapt feedfoward and feedback forces as well as their impedance in order to learn unstable tasks in daily life. According to [69.123], the principles of motor learning are:

1. Motor commands to perform a desired action are composed of both feedforward commands, defined as the component of the motor command learned by repeating an activity, and feedback commands.
2. Learning is performed in muscle space.
3. Feedforward increases with the muscle stretch in previous trial.
4. Feedforward also increases with antagonist muscle stretch.
5. Feedforward decreases when the error is small.

Mathematically, these principles can be expressed as follows [69.106]. Generally, the central nervous system tends to minimize the motion error as well as the metabolic cost such that no extra effort will be spent on the learned impedance and feedforward torques. This can be expressed by minimizing the joint-level cost function

$$V(t) = \frac{1}{2}\int_{t-T}^{t} \tilde{\boldsymbol{\Phi}}^{\mathrm{T}}(\sigma)\mathbf{Q}^{-1}\tilde{\boldsymbol{\Phi}}(\sigma)\mathrm{d}\sigma + \frac{1}{2}\boldsymbol{\epsilon}(t)^{\mathrm{T}}\mathbf{M}(\boldsymbol{q})\boldsymbol{\epsilon}(t). \tag{69.18}$$

Therein, $\mathbf{Q}$ is a positive definite weighting matrix corresponding to the learning rates; $\tilde{\boldsymbol{\Phi}}$ is defined as the difference between the instantaneous value

$$\boldsymbol{\Phi} = \left[\mathrm{vec}(\mathbf{K}_q(t))^{\mathrm{T}}, \mathrm{vec}(\mathbf{D}_q(t))^{\mathrm{T}}, \boldsymbol{\tau}_{\mathrm{ff}}(t)^{\mathrm{T}}\right]^{\mathrm{T}} \tag{69.19}$$

and the required optimal value $\boldsymbol{\Phi}^*$, that is, $\tilde{\boldsymbol{\Phi}} = \boldsymbol{\Phi} - \boldsymbol{\Phi}^*$. The quantities $\boldsymbol{\epsilon}$, $\mathbf{K}_q$, $\mathbf{D}_q$, and $\boldsymbol{\tau}_{\mathrm{ff}}$ denote the tracking control error [69.124] and the values to be learned, namely, the closed loop joint space stiffness, damping, and feed forward motor torques. For the joint stiffness adaption law, this leads for example to

$$\begin{aligned}\delta\mathbf{K}_q(t) &= \mathbf{K}_q(t) - \mathbf{K}_q(t-T)\\ &= \mathbf{Q}_{\mathbf{K}_q}\left[\boldsymbol{\epsilon}(t)\boldsymbol{e}(t)^{\mathrm{T}} - \gamma(t)\mathbf{K}_q(t)\right],\end{aligned} \tag{69.20}$$

where $\gamma(t) > 0$ is a constant forgetting factor and $\mathbf{Q}_K$, which is contained in $\mathbf{Q}$, is a symmetric positive definite matrix corresponding to the learning rate of the stiffness. T is a time constant to denote task: periodicity. In an analog manner, adaption for feedforward torque and damping can be deduced, which results in the following control law,

$$\begin{aligned}\boldsymbol{\tau}_{\mathrm{C}}(t) &= \boldsymbol{\tau}_{\mathrm{ff}}(t) - \mathbf{K}_q(t)\boldsymbol{e}(t) - \mathbf{D}_q(t)\dot{\boldsymbol{e}}(t)\\ &\quad - \mathbf{L}(t)\boldsymbol{\epsilon}(t) + \boldsymbol{\tau}_{\mathrm{r}}(t) \qquad (69.21)\\ \boldsymbol{\epsilon} &= \dot{\boldsymbol{e}}(t) + \kappa\boldsymbol{e}(t)\,, \qquad (69.22)\end{aligned}$$

where $\boldsymbol{\tau}_{\mathrm{r}}(t)$ compensates for robot/arm dynamics and bounded noise. The term $\mathbf{L}(t)\boldsymbol{\epsilon}(t)$ ensures a certain stability margin. The overall control law flow chart is depicted in Fig. 69.17. A stability proof of this approach can be found in [69.106]. An open problem with this method that remains to be unsolved is how to automatically select the meta parameters, such as the forgetting factor γ. A similar approach was developed in [69.125], where impedance adaptation laws were tested on a two-robot collaboration task. The robots lift together a beam after a task model was learned. A different approach based on the perturbations of the robot imposed kinesthetically by a human teacher such that the stiffness of the robot is adapted is investigated in [69.126]. Finally, the so-called teleimpedance paradigm [69.127] aims to remotely controlling the robot via the human arm reference position and impedance.

Learning task trajectories has been a rather well-studied field for several years now. For example, in [69.128], the authors examined the task of learning collaborative lifting of an object using hidden Markov models (HMM) and Gaussian mixture regression. Task demonstration was done via a haptic interface that controlled the robot hand. HMMs are also used in [69.129] in order to learn semantic task structures during a joint task execution. A semantic label of recognized task segments is acquired from a human partner by using speech recognition. Tasks in pHRI where transitions from contact to noncontact situations arise have been examined in [69.130]. Therein, marker data is used to obtain motion primitives. These are then updated with contact time information, comprising a low-level layer of learning. In addition, there is a high-level layer, which selects

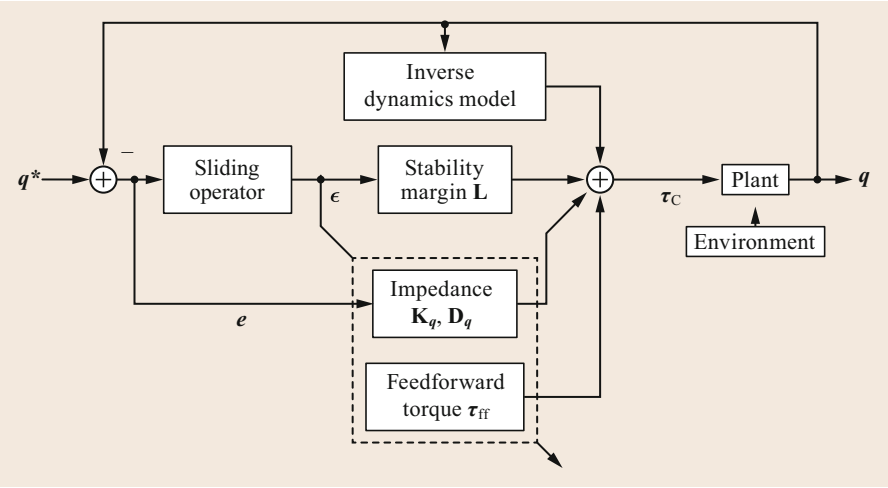

Fig. 69.17 Control diagram of the biomimetic adaptive impedance controller from (after [69.106])

a motion primitive and an end-effector reference position. Again, both layers are encoded via HMMs to provide a suitable abstraction, which is a key when dealing with high-dimensional spaces.

In [69.17], dimensionality reduction for learning was employed to realize assistive tasks, such as helping a robot to stand–up or walk. This principal component analysis (PCA)-based reduction lets the learning take place in a low-dimensional joint manifold instead of the original high-dimensional space. It reduces the complexity of the learning domain for multidegree-of-freedom systems such as humanoids. A recent approach to learning trajectories based on human preferences was proposed in [69.131], where machine-learning techniques were applied to derive the optimal behavior from human action ratings during runtime. Figure 69.18 shows how the robot learns to handle a knife safer by receiving low rewards from the human if the dangerous tool is moved in undesired orientations and/or trajectories.

69.4.3 Collision Handling

One of the core problems in pHRI is the handling of collisions between robots and humans, with the primary motivation of limiting possible human injury due to physical contacts. Various *monitoring signals* can be used to gather context independent information about the event.

The *collision detection phase*, whose binary output denotes whether a robot collision occurred or not, is characterized by the transmission of contact wrenches, often for very short impact durations. The occurrence of a collision, which may happen anywhere along the robot structure, shall be detected as fast as possible. A major practical problem is the selection of a threshold on the monitoring signals, so as to avoid false positives and achieve high sensitivity at the same time. A heuristic approach is to monitor the measured currents in robot electrical drives, looking for fast transients possibly caused by a collision [69.132, 133]. Another proposed scheme compares the actual commanded torques (or motor currents) with the nominal model-based control law (i. e., the instantaneous torque expected in the absence of collision), with any difference being attributed to a collision [69.134]. This idea has been refined by considering the use of an adaptive compliance control [69.135, 136]. However, tuning of collision detection thresholds in these schemes is difficult because of the highly varying dynamic characteristics of the control torques.

Knowing which robot part (e.g., which link of a serial manipulator) is involved in the collision is an important information that can be exploited for robot

Fig. 69.18 The robot Baxter learns to safely handle a knife ([69.131]; courtesy of Saxena's Robot Learning Lab)

reaction. *Collision isolation* aims at localizing the contact point $\boldsymbol{x}_c$, or at least which link i_c out of the n-body robot collided. One way to obtain both collision detection and isolation is to use sensitive skins [69.92–95]. However, it would obviously be more practical and reliable to detect and possibly isolate a collision without the need of additional tactile sensors. On the other hand, the previously mentioned monitoring signals used in [69.132–136] are in general not able to achieve reliable collision isolation (even when robot dynamics is perfectly known). In fact, they either rely on computations based only on the nominal desired trajectory, or compute joint accelerations by inverting the mass matrix and thus spreading the dynamic effects of collision on a single link, or use acceleration estimates for torque prediction and comparison, which inherently introduces noise (due to double numerical differentiation of position data) and intrinsic delays. The common drawback of these methods is that the effect of a collision on a link propagates to other link variables or joint commands due to robot dynamic couplings, thus affecting the isolation property.

Other relevant quantities about a collision that are deduced during the *collision identification phase* are the directional information and the intensity of the generalized collision force, either in terms of the acting Cartesian wrench $\boldsymbol{\mathcal{F}}_{\text{ext}}(t)$ at the contact, or of the resulting joint torque $\boldsymbol{\tau}_{\text{ext}}(t)$ during the entire physical interaction event. This information characterizes (in some cases, completely) the collision event. The first method that simultaneously achieved collision detection, isolation, and identification was proposed in [69.137]. The basic idea was to view collisions as faulty behaviors of the robot actuating system, while the detector design took advantage of the decoupling property of the robot *generalized momentum* $\boldsymbol{p} = \mathbf{M}(\boldsymbol{q})\dot{\boldsymbol{q}}$ [69.138, 139].

During the *collision reaction phase*, the robot should react purposefully in response to a collision event, that is, taking into account available contextual information. Because of the fast dynamics and high uncertainty of the problem, the robot reaction should be embedded in the lowest control level. For instance, the simplest reaction to a collision is to stop the robot. However, this may possibly lead to inconvenient situations, where the robot is unnaturally constraining or blocking the human [69.19]. To define better reaction strategies, information from collision isolation, identification and classification phases should be used. Some examples of successful collision reaction strategies have been given in [69.88, 140].

Collision Detection and Identification

A recent overview on standard techniques to estimate $\boldsymbol{\tau}_{\text{ext}}$ can be found in [69.26]. In this chapter, we focus on the main method, namely the monitoring method based on the observation of the generalized momentum that was introduced in [69.137]. The scheme, which is regarded as the standard algorithm, was motivated by the desire of avoiding the inversion of the robot inertia matrix, decoupling the estimation result, and also eliminating the need of an estimate of joint accelerations. The according disturbance observer-based estimator for the rigid case is defined as

$$\boldsymbol{r}(t) = \mathbf{K}_{\text{O}} \left\{ \hat{\boldsymbol{p}}(t) - \int_0^t [\boldsymbol{\tau} - \hat{\boldsymbol{\beta}}(\boldsymbol{q}, \dot{\boldsymbol{q}}) + \boldsymbol{r}] \mathrm{d}s - \hat{\boldsymbol{p}}(0) \right\} , \tag{69.23}$$

with $\hat{\boldsymbol{p}} = \hat{\mathbf{M}}(\boldsymbol{q})\dot{\boldsymbol{q}}$, $\hat{\boldsymbol{\beta}}(\boldsymbol{q}, \dot{\boldsymbol{q}}) = \hat{\boldsymbol{g}}(\boldsymbol{q}) + \hat{\boldsymbol{C}}(\boldsymbol{q}, \dot{\boldsymbol{q}})\dot{\boldsymbol{q}} - \dot{\hat{\mathbf{M}}}(\boldsymbol{q})\dot{\boldsymbol{q}}$, and $\mathbf{K}_{\text{O}} = \text{diag}(k_{\text{O},i}) > 0$ being the diagonal gain matrix of the observer. Under ideal conditions, $\hat{\mathbf{M}} = \mathbf{M}$ and $\hat{\boldsymbol{\beta}} = \boldsymbol{\beta}$, the dynamic relation between the external torque $\boldsymbol{\tau}_{\text{ext}}$ and $\boldsymbol{r}$ is

$$\dot{\boldsymbol{r}} = \mathbf{K}_{\text{O}}(\boldsymbol{\tau}_{\text{ext}} - \boldsymbol{r}) . \tag{69.24}$$

In other words, $\boldsymbol{r}$ is a stable, linear, decoupled, first-order estimation of the external collision torque $\boldsymbol{\tau}_{\text{ext}}$. Large values of $k_{\text{O},i}$ give small time constants $T_{\text{O},i} = 1/k_{\text{O},i}$ in the transient response of that component of $\boldsymbol{r}$, which is associated with the same component of the external joint torque $\boldsymbol{\tau}_{\text{ext}}$. In the limit, we obtain

$$\mathbf{K}_{\text{O}} \to \infty \quad \Rightarrow \quad \boldsymbol{r} \approx \boldsymbol{\tau}_{\text{ext}} . \tag{69.25}$$

Collision Reflex Reactions

After a collision has been detected, suitable collision reflex reaction is needed. Four basic context-independent joint-level collision reflexes are discussed next. They lead to significantly different reflex behavior after a contact was detected. In the third and fourth schemes, the directional information on contact torques provided by suitable identification schemes such as (69.23) may be used to safely drive the robot away from the collision location.

Robot Stop. The most obvious strategy to react to a collision is to stop the robot. This behavior can, for example, be obtained by setting $\boldsymbol{q}_{\text{d}} = \boldsymbol{q}(t_c)$, where t_c is the instant of collision detection or by simply engaging the robot's brakes. More elaborate braking strategies can be found in [69.141].

Torque Control with Gravity Compensation. One may also react to a collision by switching the controllers. Typically, prior to the collision incident, the

robot moves along a desired trajectory with a position reference-based controller (e.g., position or impedance control). After detection, the control mode is switched to a compliance-based controller that ignores the previous task trajectory. A particularly useful variant is to switch to torque control mode with gravity compensation $\boldsymbol{\tau} = \hat{\boldsymbol{g}}(\boldsymbol{q})$ (VIDEO 611). Note that this strategy does not explicitly take into account any information about $\boldsymbol{\tau}_{\text{ext}}$.

Torque Reflex. This strategy extends the torque control-based strategy by explicitly incorporating the estimation or measurement of $\boldsymbol{\tau}_{\text{ext}}$ into the motor torque $\boldsymbol{\tau}$ via

$$\boldsymbol{\tau} = \hat{\boldsymbol{g}}(\boldsymbol{q}) + (\mathbf{I} - \mathbf{K}_{\text{r}})\boldsymbol{\tau}_{\text{ext}} \,, \tag{69.26}$$

where $\mathbf{K}_{\text{r}} = \text{diag}\{k_{\text{r},i}\} > 1$. It can be shown that, under sufficiently accurate estimates or measurements, such a law is equivalent to scaling of the robot dynamics by $\mathbf{K}_r^{-1}$. The closed-loop dynamics become

$$\underbrace{\mathbf{K}_r^{-1}\mathbf{M}(\boldsymbol{q})}_{\mathbf{M}'(\boldsymbol{q})}\ddot{\boldsymbol{q}} + \mathbf{K}_r^{-1}\mathbf{C}(\boldsymbol{q}, \dot{\boldsymbol{q}})\dot{\boldsymbol{q}} + \boldsymbol{\tau}_{\text{ext}} = \mathbf{0} \,, \tag{69.27}$$

where $\mathbf{M}(\boldsymbol{q}) > \mathbf{M}'(\boldsymbol{q})$ holds component-wise.

Admittance Reflex. Reference trajectory modification via an admittance-type strategy that uses the measurement or estimation of $\boldsymbol{\tau}_{\text{ext}}$ can easily, for example, be realized via

$$\boldsymbol{q}_{\text{d}}(t) = -\int_{t_{\text{c}}}^{\text{T}} \mathbf{K}_{\text{a}}\boldsymbol{\tau}_{\text{ext}}\, \text{d}t \,, \tag{69.28}$$

where $\mathbf{K}_{\text{a}} = \text{diag}\{k_{\text{a},i}\} > 1$. With this scheme that requires no control switching the robot quickly drives away from the external torque source and decreases the contact forces till they decay to zero.

69.4.4 Shared Manipulation Control

Collaborative carrying, particularly of a long, large, heavy or flexible object, is a common scenario in pHRI research (Fig. 69.19). As discussed earlier, Cobots represent the parallel case where passive robotic devices control the path along which a shared load will be transported, but give their operator full control of load motion along that path (Chaps. 39 and 70; VIDEO 821). Most shared manipulation schemes utilize some form of impedance control [69.143]. In an early work, the authors of [69.144, 145] proposed an impedance controller with speed-dependent damping coefficients. The authors of [69.146] employed a similar approach (with fixed virtual impedance) to control the horizontal movement of their Mobile Robot Helper's mobile base in response to applied forces of a human user on the other end of a cooperatively carried load (VIDEO 606). The authors of [69.145] also described a lifting controller employing a pair of cascaded second-order virtual admittance controllers. Due to the raising/lowering of a cooperatively carried load the applied torques on an admittance-controlled, high-stiffness wrist generate a wrist deflection that translated (via a fixed gain) into a virtual vertical force. This force raised or lowered the robot end effector via a second admittance controller. In [69.142], an admittance controller was presented that was tuned for human preference, which is typically slightly underdamped. In [69.147], an admittance strategy was used to translate user force input into robot steering commands within a constrained trajectory.

Ideally, in cooperative manipulation, robotic and human partners will naturally take turns with leading and following roles depending on the state of a shared task. A switching model for haptically linked human–robot pairs that allows the robot to continuously vary its behavior from *completely following* to *completely leading* was introduced in [69.16]. In [69.148], the authors presented a mathematical treatment of the cooperative load manipulation problem to allow one or more robots to carry a load with a human user along a desired trajectory. They also incorporated variable leading behavior in the robots, enabling them to just steer the load (following) or completely control the load's axial motion (leading).

More recently, Evrard's homotopy approach was applied to load lifting, enabling the robot assistant to vary its behavior between leading and following based on its confidence in its predictions of the human user's

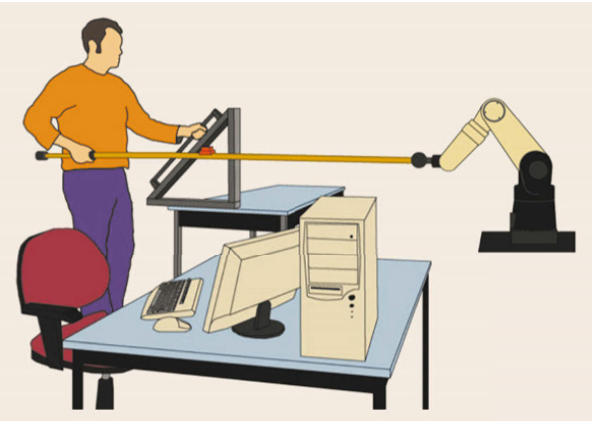

Fig. 69.19 Collaborative lifting experiment with a long object (after [69.142])

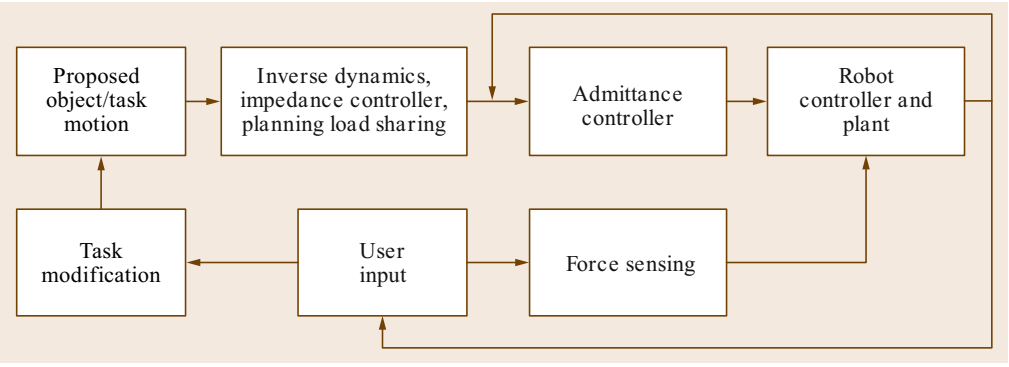

Fig. 69.20 Generalized schematic for collaborative task control

intentions [69.15] (VIDEO 617). These are monitored through the kinematics of the shared load. Recently, an admittance control law that guarantees the stability of the robot during constrained motion and also provides a quite intuitive human interaction was designed in [69.149]. The admittance law uses the time derivative of the contact force between the human and the robot to estimate human intent and an online estimate of the interaction stiffness resulting in very accurate shared-control of the robot system. In [69.150], the authors developed and user tested an interactive controller for a collaborative carrying task, utilizing a strategy to model effort sharing between the robot and the user. A generalized schematic for admittance-based collaborative task control is depicted in Fig. 69.20. On the motion planning side, minimum jerk trajectories [69.151] have been used to generate robot trajectories that are well matched to the motion of the human partner, and require the human to use less energy in the interaction, for example, [69.152]. Results from [69.153] indicate that a simpler quintic trajectory was also suitable for this purpose.

69.5 Motion Planning for Human Environments

The definition and quantification of injury, pain, or general risk are essential to express what safe behavior really means. The according insights can also be applied to generate safer robot motions such that injury and risk prevention are explicitly taken into account at this level. Two main branches of motion planning algorithms for danger reduction were developed, which are described hereafter.

69.5.1 Biomechanically Safe Motion Planning

As mentioned in the beginning of the chapter, human collision safety has to be ensured from an injury biomechanics perspective. Safety could, for example, be defined as *ensuring that only mild contusions may occur in worst case scenarios*. The natural question that arises is now how to formally respect such a metric, that is, how should a robot be controlled so that an unforeseen contact remains subcritical according to the underlying injury biomechanics or pain data. For this the authors of [69.25] gave the schema, termed safe motion unit (SMU), to link basic data to intrinsically safe robot velocity. The basic idea is to represent any data or general insight in a (possibly purely data driven) functional relation, linking impact properties to human injury or pain. With this, it is possible to calculate the instantaneous safe robot velocity given the robot's inertial properties, surface curvature, and possible human body parts it might collide with

$$(\text{mass}, \text{velocity}, \text{geometry}, \text{body part}) \rightarrow \text{observed injury/pain}\,. \tag{69.29}$$

For the injury/pain metric, multiple international classifications exist from which one may choose from. In [69.25], for example, the AO-classification was used. Thereafter, a careful set of experiments, or if possible simulations, can be generated to deduce the relation of interest. Each experiment should be designed such that the impacting mass, its velocity, and curvature are known in addition to any supplementary sensory readings of interest. Furthermore, the observed, measured, or calculated injury and/or pain level of the involved body part has to be quantified according to the selected scale. To restrict the amount of experiments to a feasible number, the impactor geometry is assumed to be composed of different basic geometric primitives (spheres, cuboids, corners). Thus, a finite set of so-called *safety curves* can be constructed, which represent fitted threshold curves for a given injury indicator in

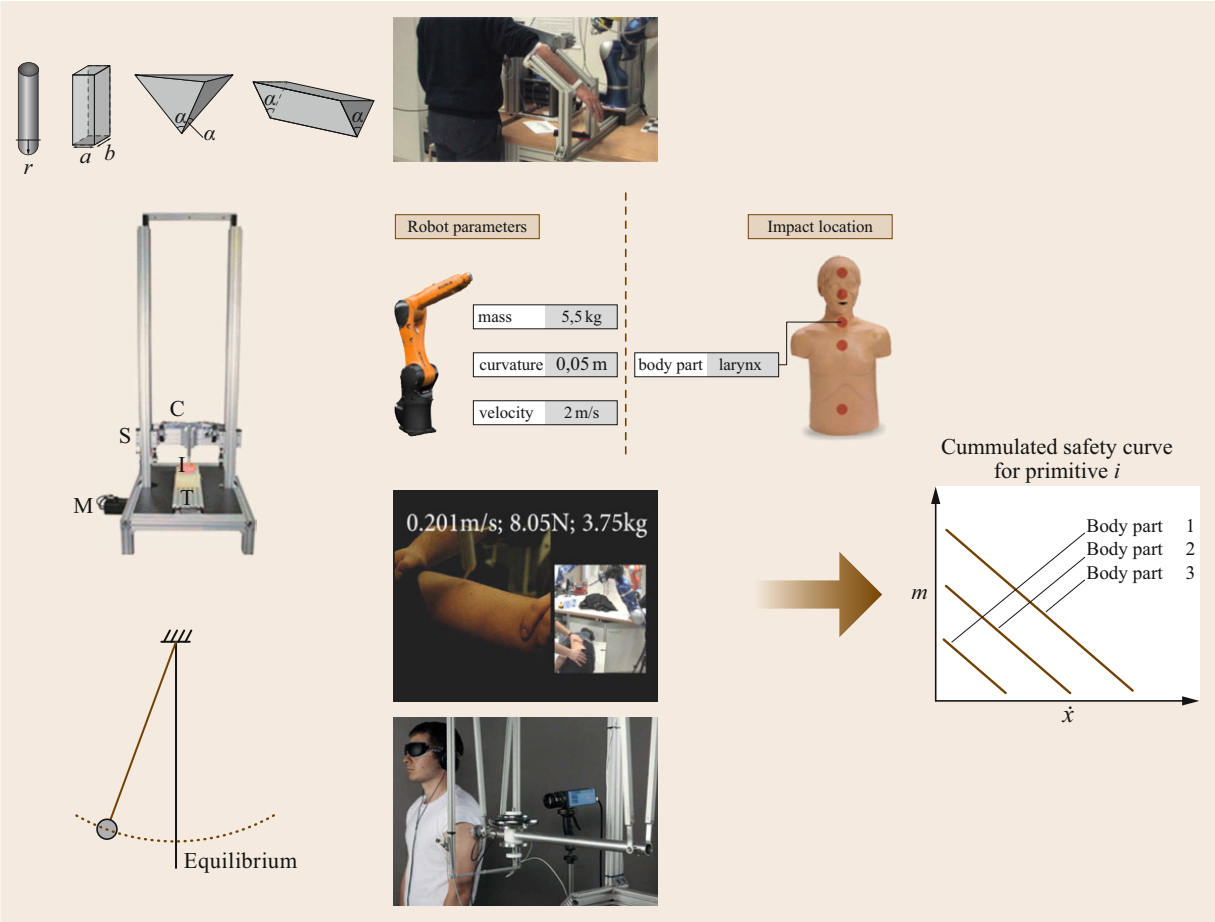

Fig. 69.21 A unified view: From collision experiment/simulation to cumulative *safety curves* for biomechanically safe robot velocity. Copyright of the bottom photograph: Fraunhofer IFF (www.iff.fraunhofer.de)

the mass–velocity space parameterized by the body part (Fig. 69.21).

This idea can now be applied to a robot for safe velocity generation (Fig. 69.22). The concept is to scale any desired velocity command $\dot{\boldsymbol{q}}_\mathrm{d}$ by α to a biomechanically safe value $\dot{\boldsymbol{q}}_\mathrm{d}^*$. The scalar α is computed from evaluating the instantaneous robot inertial and local surface properties with respect to their injury potential. For this, the effective mass m_POI in the respective $\boldsymbol{u}$-directions of the relevant points of interest (POIs) are

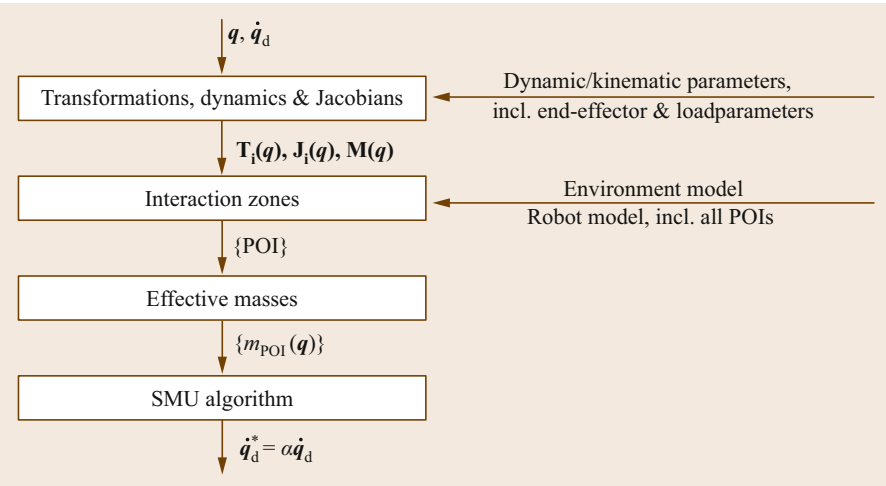

Fig. 69.22 Pipeline for creating biomechanically safe velocities based on the SMU algorithm (after [69.25])

evaluated via (69.7). Each POI is associated with a surface geometry primitive that is then used to link the respective POI to some underlying biomechanical injury, pain, or risk *safety curve*.

69.5.2 Risk-Metric-Based Motion Planning

As discussed in Sect. 69.4.3, there are numerous techniques for detecting impacts or potential collisions during pHRI. Collision monitoring methods can be used to ensure that forces and torques, or more simply the energy, of the robot system are limited during a collision event. To ensure safe and human-friendly interaction in unstructured environments, additional safety measures, utilizing system control, and planning are required.

Since physical interaction itself is a collision, a key problem of human-safe planning and control methods is to identify when human safety is actually threatened. In [69.155], a danger evaluation method was developed using the potential impact force as an evaluation measure. In this work, several danger indices were proposed based on the design properties of the robot. This danger index can be defined as a product of factors which affect the potential impact force between the robot and the human, such as distance, relative velocity, robot inertia, and robot stiffness. The authors applied this index as an objective function for improved mechanical design, control, and motion planning. A danger index based on estimated impact forces for a potential collision between a robot and a human was computed in [69.156] and used as an input to a real-time trajectory generation system, which balances the goal seeking with potential danger. In [69.154], the same authors combined their system with a vision based and physiological monitoring system, which allows the robot to respond to the user's real-time position and attentiveness. During the interaction, the user is monitored to asses his level of approval of the robot's actions while the trajectory planner monitors safety factors, such as robot velocity and user intent. Finally, the safety control module provides a real-time response to short-term horizon factors evaluated by a *safety measure estimation module* (Fig. 69.23).

For mobile service robots, the authors of [69.157] proposed a collision avoidance controller based on estimates of user behavior, using a *social force* model to determine whether the user intends to avoid the collision or not so that the robot can respond accordingly. In [69.158], the authors introduced a method using so-called kinetostatic danger fields as a metric for the danger which the current posture and velocity of a robot pose to objects in its environment. The work presented in [69.122] shows an algorithm which maximizes the productivity of an industrial robotic manipulator while guaranteeing a safe human–robot distance. In addition to the relative human–robot distance, it takes also dynamic and control characteristics into account. In [69.159], the authors proposed a method based on an intuitive physical interpretation, namely, an impedance-like second-order motion generation. It is designed to provide safe motion in complex environments, taking into account both proximity to objects, and external forces. A method that achieves collision avoidance for a redundant robot while permitting the end-effector task to continue is presented in [69.160]. Using data from a 3-D-RGB-D camera, this method is purely based on computations of distances between the robot body and dynamic obstacles in the workspace (e.g., the user) that are processed through a *risk function* to adjust the joint

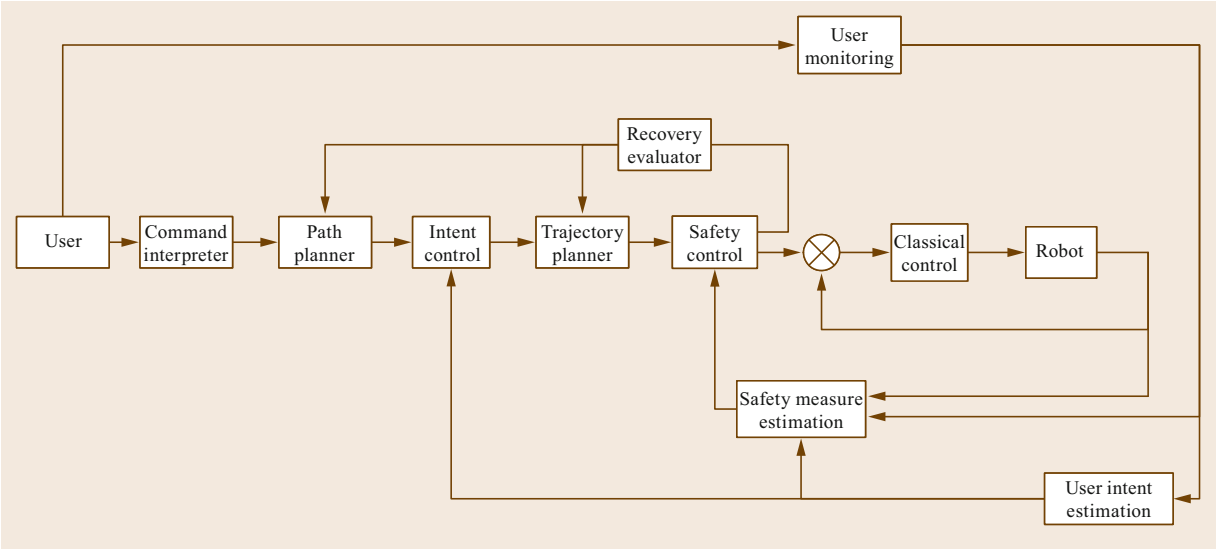

Fig. 69.23 Schematic of motion planning system with user intent and safety monitoring input (after [69.154])

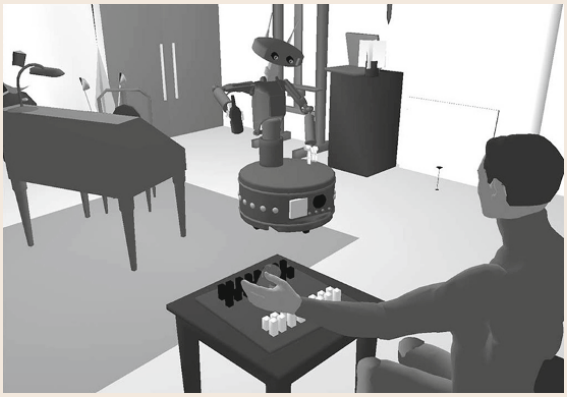

Fig. 69.24 Human-aware motion planner of Laboratoire d'analyse et d'architectures des systèmes (LAAS) (after [69.161]; courtesy of Rachid Alami)

velocities. The motion task of the end effector is modified by an artificial potential field-type method.

69.5.3 Human-Aware Motion Planning

Applying and extending classical motion planning techniques to the problem of human-robot interaction was originally done in [69.161]. The authors developed a human aware mobile robot motion planner, which incorporates humans accessibility, their vision field, and their preferences in terms of relative human–robot placement (Fig. 69.24). Human dynamics were integrated into the algorithm.

Extensions of the original work toward a motion planner for pHRI scenarios were elaborated in [69.162]. Therein, certain constraints, such as distance, visibility, and comfort are taken into account to generate safer motions and were demonstrated within a handover scenario. The algorithm has been extended to cluttered environments in [69.163], where a randomized cost-based exploration method provides an initial path that is relevant with respect to pHRI and workspace constraints.

69.6 Interaction Planning

In order to profit from the collaboration of human and robot by combining the flexibility, knowledge and sensory skills of a human with the efficiency, strength, endurance, and accuracy of a robot, according interaction planners need to be designed to plan their joint actions for a common goal. In the interaction planning domain, the central question is how to plan robot human joint actions and reactions in a certain interaction process, involving also unexpected environmental changes, one of the most basic ones being the human entering the robot's workspace. The definition of the interaction planning problem and the integration of reflex reaction schemes that potentially lead to an abrupt deviation from nominal course have to be elaborated. On an architectural level, the incorporation of *reactivity* has to be systematically represented.

69.6.1 Collaborative Action Planning

Approaches to subproblems of the full interaction planning problem were addressed in the literature. In [69.164], for example, the system SHARY for human-aware task planning was introduced. It produces social plans of a task by implementing communication schemes to negotiate the task solution with the human partner.

In [69.165], dynamic neural fields (DNFs) were used to build a decision-making system for interaction in cooperative human–robot tasks. The main idea is to let the robot imitate human behavior in order to make the cooperation between robot and human appear rather intuitive. A structural overview of the system is depicted in Fig. 69.25. A vision system observes the scenery and recognizes task-related objects and gestures of the human coactor. Object positions are stored in the *object memory layer*. The *action observation layer* decides which type of known action was executed by the coactor. The expected outcome of this action is then simulated by the *action simulation layer* and thereafter passed to the *intention layer*. Here, the intention of the coactor is determined. The knowledge about the coactor's intention and the expected outcome of his actions is used by the *common subgoal layer*. It contains prior knowledge about the task structure and the subgoals to be achieved for task completion. The *common subgoal layer* is responsible for enabling actions that lead to the fulfillment of a currently achievable subtask only. Based on the information coming from the *intention layer* and the *object memory layer*, the *action execution layer* decides to perform an action, which supports the human in the intended subtask or leads to the completion of an independent subtask and does not interfere with the current human intention. Each layer of the system is formalized by one or more DNFs. The activity $u_i(x, t)$ at time t of a neuron x is described by the differential

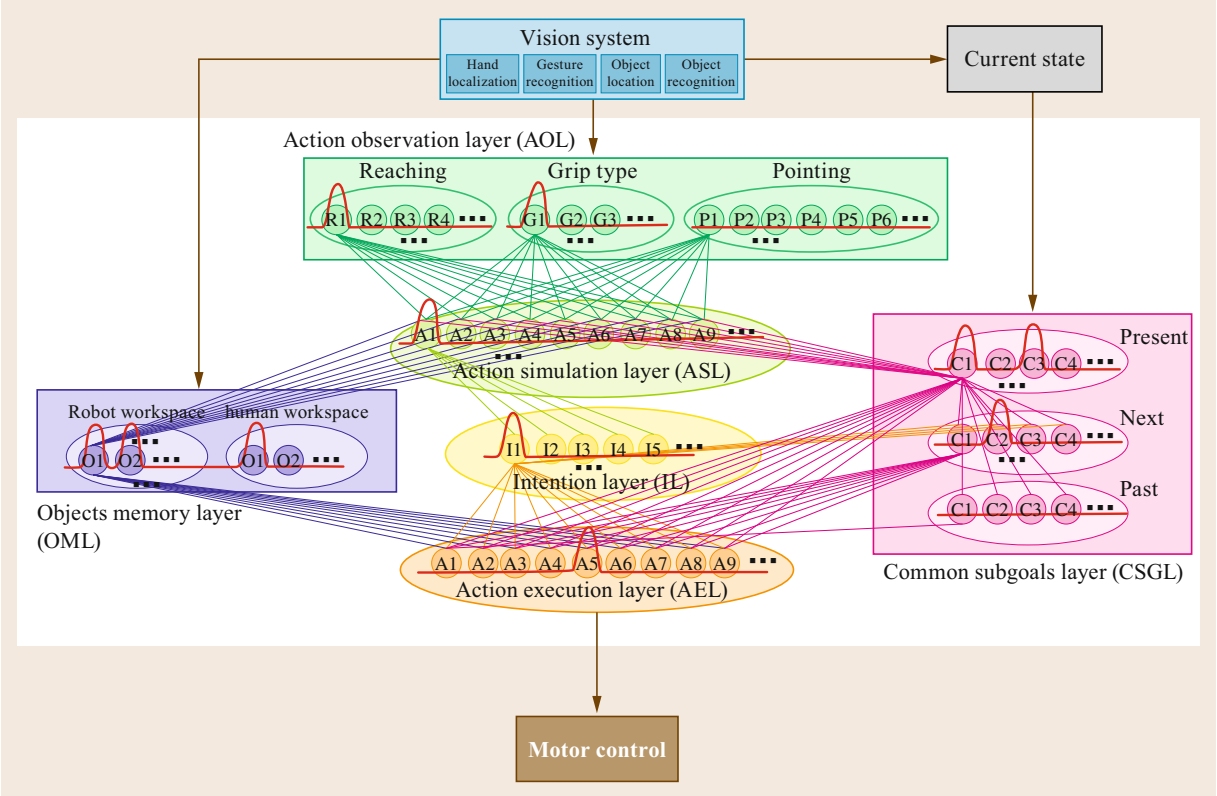

Fig. 69.25 Structural overview of the decision-making system from (after [69.165]; courtesy of Estella Bicho)

equation

$$\tau_i \frac{\delta u_i(x,t)}{\delta t} = -u_i(x,t) + S_i(x,t) + \int w_i(x-x') f_i(u_i(x',t))\mathrm{d}x' - h_i \,, \tag{69.30}$$

where $\tau_i > 0$ and $h_i > 0$ denote the timescale and the resting level of the field dynamics, respectively. S_i is the summed input to a local population. The output function f_i is chosen to be a sigmoid function and the interaction strength $w_i(x-x')$ is a Gaussian curve, which depends only on the distance between x and x' (Fig. 69.26).

In [69.130], a mimetic communication model for pHRI is introduced, where the according motion primitives are taught by human demonstration via marker control. These are subsequently encoded into hidden Markov models (HMMs) and allow the robot to execute them and even to recognize the motion primitives executed by the human partner. Based on the motion primitives, interaction primitives are then learned as chains of actions and reactions. The flow of interaction primitive learning is depicted in Fig. 69.27a. First, the robot executes a motion primitive, followed by observing the human's respective reaction in order to learn the correct interaction pattern sequence. After this step, the motion primitives are updated and the process is repeated. The underlying scheme of interaction is shown in Fig. 69.27b. The learned motion primitives are encoded as continuous HMMs (CHMMs) and form the middle layer of the system. They are then used to recognize the motion primitive executed by

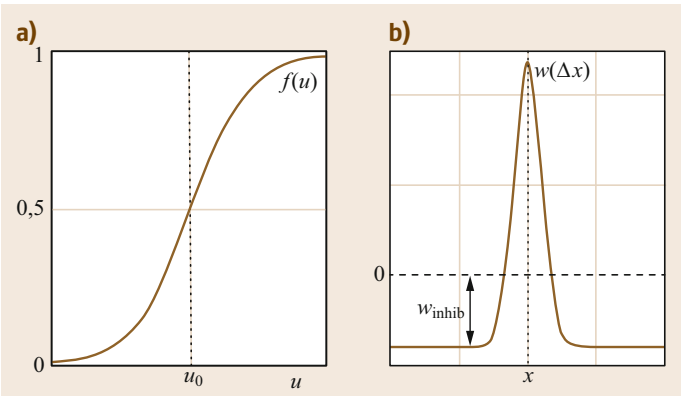

Fig. 69.26 **(a)** Nonlinear threshold output function that maps activity to a sigmoidal with threshold u_0. **(b)** Synaptic weight function for modeling the interaction strength between any two neurons x and x' in (69.30) (after [69.165]; courtesy of Estella Bicho)

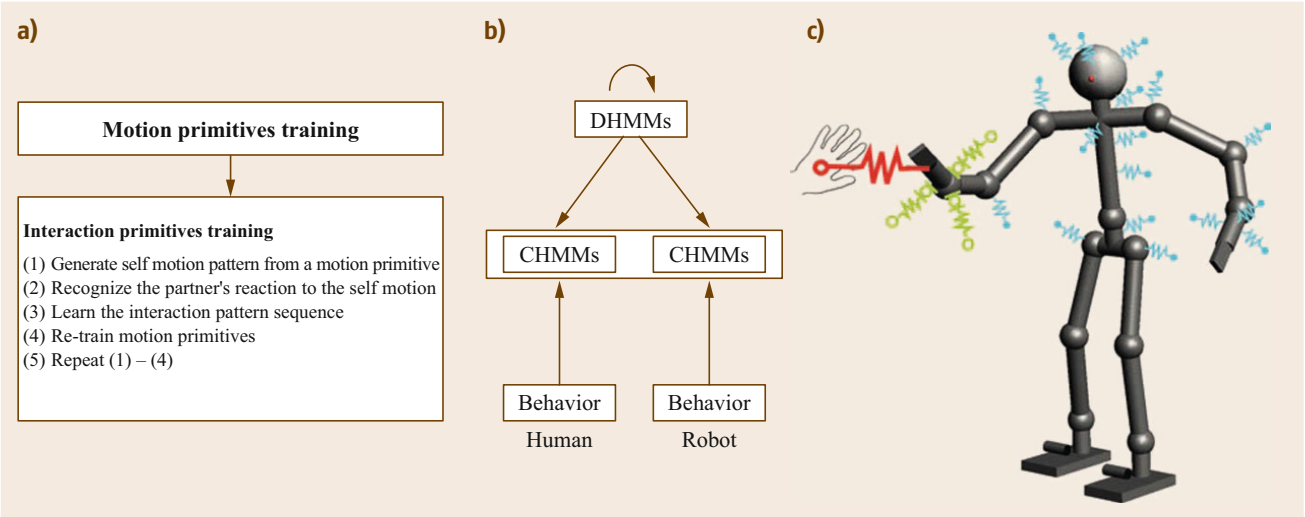

Fig. 69.27 (a) Learning of interaction primitives. (b) Scheme of interaction. (c) Adaption of robot motion via virtual spring (after [69.130]; courtesy of Dongheui Lee)

the human and to generate the motion of the robot according to the interaction primitives encoded as discrete HMMs (DHMMs) at the top. The robot motion (more precisely its behavior in the context of the authors' work) may then be modified to adapt to human motion in the real world (expressed by the thin horizontal arrow). The bold horizontal arrow represents the assumed adaption of the human to the robot behavior. The adaptation strategy of the robot movement is depicted in Fig. 69.27c. For this, an impedance controller is used in combination with a virtual spring connected to the robot hand to attract the device into the correct position. Figure 69.28 depicts an application of the interaction scheme, where the robot high- or low-fives a human coactor with one or two hands, respectively.

69.6.2 Interaction Planning Problem

In order to formalize the interaction planning problem, one needs to be able to describe the entire scenario, the system state of the robot, the state of the human(s) (possibly including future behavior prediction of both), the environment state including all relevant objects and the overall abstract task state. This information about the world state comprises the concept of an *interaction world*, which builds the basis for formulating the general *interaction planning problem*.

Definitions

The set of *world states* $\boldsymbol{WS}$ is defined as

$$\boldsymbol{WS} = \boldsymbol{RS} \times \boldsymbol{HS}^n \times \boldsymbol{OBS}^m \times \boldsymbol{TS}\,, \tag{69.31}$$

where $\boldsymbol{RS}, \boldsymbol{HS}, \boldsymbol{OBS}, \boldsymbol{TS}$ denote the set of the robot states, n humans, m obstacles, and an overall task state, respectively.

The set of *robot states*

$$\boldsymbol{RS} = \boldsymbol{S} \times \boldsymbol{RA}^n \times \boldsymbol{IR} \tag{69.32}$$

contains information about the internal state $s \in \boldsymbol{S}$ of the robot, the robot awareness $ra \in \boldsymbol{RA}$, and the interaction state $ir \in \boldsymbol{IR}$. The interaction state of the robot may, for example, take the values *autonomous*, *collaborative*, or *cooperative*. The robot awareness indicates its ability to predict human actions. The set of internal states $\boldsymbol{S} = \boldsymbol{S}_{\text{ac}} \times \boldsymbol{S}_{\text{b}} \times \boldsymbol{S}_{\text{p}}$ contains information about the set of actions carried out by the robot $\boldsymbol{S}_{\text{ac}}$. Furthermore, the behavior set $\boldsymbol{S}_{\text{b}}$, which includes, for example, controller choices and respective parameterizations, reflex reactions, and type or parameterizations of trajectory

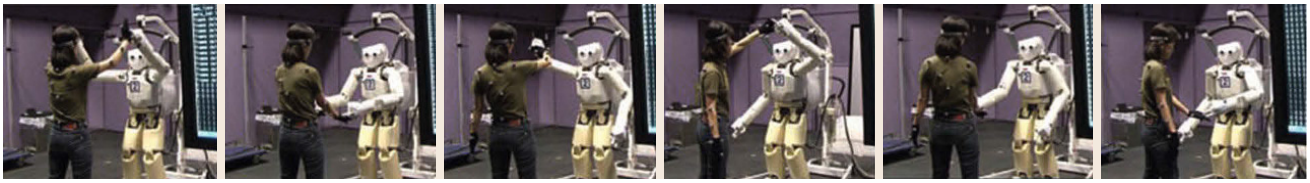

Fig. 69.28 pHRI using the mimetic communication model (after [69.130]; VIDEO 625; courtesy of Dongheui Lee)

planners. Such a reflex reaction which can be thought of as an analogy to human reflexes, intends to bring the robot to a safe state or even a reflex cascade $\boldsymbol{R}$ (Sect. 69.6.3). Finally, the physical state $sp \in \boldsymbol{S}_\mathrm{p}$ contains, for example, the robot's instantaneous position, velocity, and momentum.

The set of *human states*

$$\boldsymbol{HS} = \boldsymbol{PSH} \times \boldsymbol{PA} \times \boldsymbol{HA} \times \boldsymbol{IH} \times \boldsymbol{D} \tag{69.33}$$

combines the sets of physical state $\boldsymbol{PSH}$ (position, velocity, etc.), personal attributes $\boldsymbol{PA}$ (fitness, age, experience, etc.), human awareness $\boldsymbol{HA}$ (the ability of the human to predict the robots actions), interaction states of the human $\boldsymbol{IH}$ (for example, *waiting for robot*, *work with robot* or *work without robot*), and the distances $\boldsymbol{D}$ between human and robot. In its most simple nontrivial case, $\boldsymbol{D}$ could, for example, consist of the elements *in workspace*, *in perception*, *out of perception*, and *lost perception*.

The set of *task states*

$$\boldsymbol{TS} = \boldsymbol{A} \times \boldsymbol{TC} \times \boldsymbol{IS} \tag{69.34}$$

contains $\boldsymbol{A}$, $\boldsymbol{TC}$, $\boldsymbol{IS}$ that denote the sets of possible actions, task criticality, and expected interaction between human and robot, respectively. The task criticality specifies the effect of potential task failure on human safety. A task consists of the meaningful composition of actions and/or more complex skills such as *grasp object* or simply *move to pose* according to a particular creation process.

The Interaction Planning Problem

The *interaction planning problem* then denotes the problem of selecting a suitable, and if possible optimal, robot action and associated behavior in every time step based on the information contained in the world state, the history of the process $\boldsymbol{HIS}$, and available (dynamic) knowledge stored in a knowledge base $\boldsymbol{KB}$ (for example, safety knowledge, object properties, world grounding rules, ...). Formally, this can be expressed by the *select action* mapping

$$sa : \boldsymbol{WS} \times \boldsymbol{HIS} \times \boldsymbol{KB} \rightarrow \boldsymbol{S}_\mathrm{ac} \times \boldsymbol{S}_\mathrm{b} \,. \tag{69.35}$$

Optimality could, for example, be expressed in the following *reinforcement learning* sense, where the selected behavior shall lead to a maximum reward. This is obtained as follows:

1. A *task evaluator* evaluates the suitability of a particular action/behavior for fulfilling the desired task.
2. A *safety evaluator* evaluates the overall safety of the situation by taking into account different biomechanical injury criteria, the expected interaction between human and robot, human–robot–related geometric quantities, such as minimal distance, as well as the task criticality.
3. Finally, additional rewards may be given by the human in order to capture human-friendly behavior.
4. The overall reward is then a suitable combination of the basic rewards.

69.6.3 Robot Reflexes

Human reflexes are involuntary reactive body movements in response to a perceived input, the so-called stimulus, that is, one does not even have to *think about what to do*. In humans, reflexes aim for body protection. Based on built-in heuristics, they automatically protect the human body from injury. However, the exact separation in terms of hybrid system-like theory is not yet clear. Thus, the line between discrete reflex states and according systemic responses on both electrical and mechanical levels is somewhat blurred. In robotics, on the other hand, it is possible to separate these levels and extend the concept of basic *nominal robot actions* by *reflex reactions* [69.9, 86, 140]. These concepts systematically incorporate the possibilities one gains from the already described collision detection and reflex reaction schemes (Sect. 69.4.3). Other work in similar directions for developing human-like withdrawal reflexes can be found in [69.166].

In contrast to the classical planning and execution pipeline, the activation of reflexes that are able to override the nominal task plan due to environmental or internal conditions that do not comply with nominal task behavior have to be considered. In contrast to humans, these reflexes do not necessarily have to be fixed (or slowly time-varying over learning cycles). On the contrary, they may be tailored to every nominal action such that local context dependency (in particular instantaneous sensory input) may be taken into account. After instantaneous reactions are executed, the main problem is to decide what to do next. Either local re-entry into the previous plan or entire re-planning have to be executed. Figure 69.29 depicts the overall concept also in the context of task and interaction planning.

Formally, a robot reflex is associated with a suitable activation signal. Typically, this represents either the indication of a certain stimulus or a fault. Stimuli are general perception inputs, whereas faults are detected either by processed stimuli (observation of external torques, proximity information, etc.) or general system malfunctions as, e.g., communication collapse or runtime violations. Even rather complex reflex patterns can be activated that may be represented as directed reflex graphs, i. e., a decisional component in the inner most

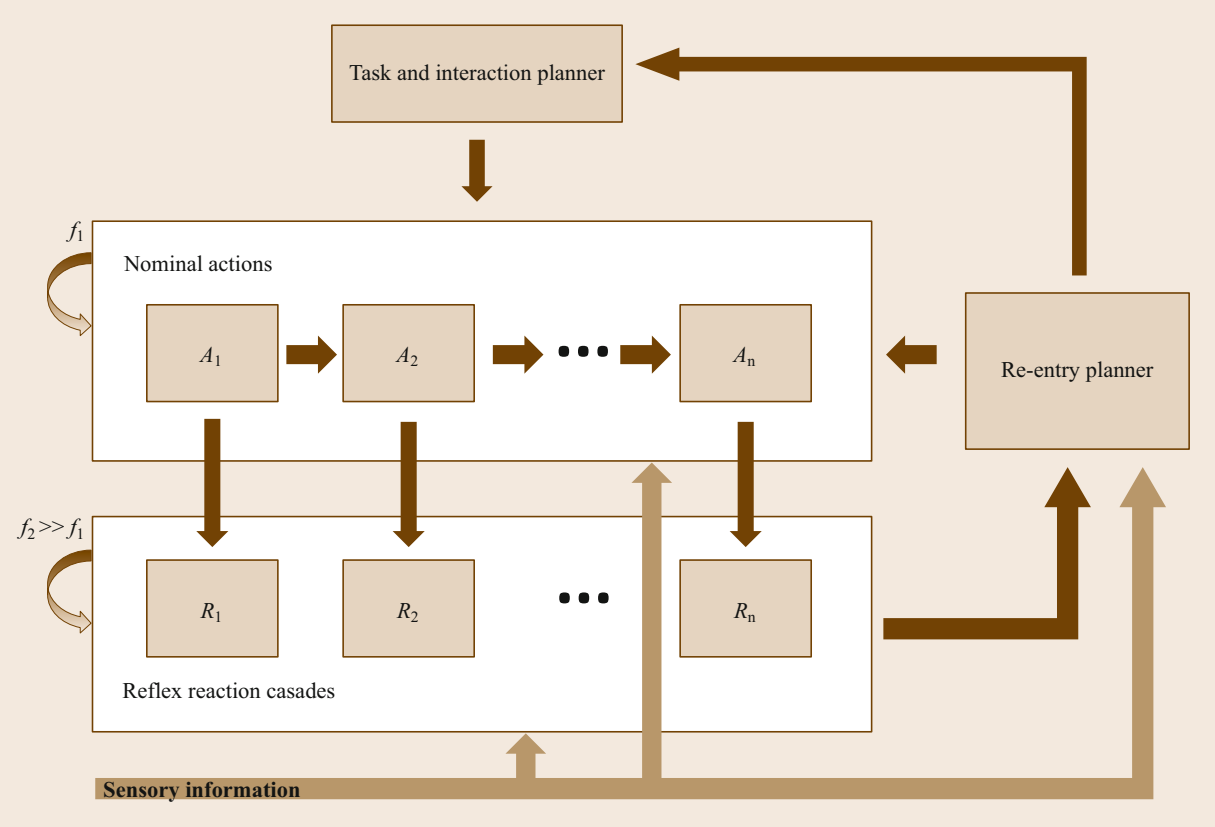

Fig. 69.29 Conceptual sketch of robot reflexes; f_1 and f_2 indicate the update rates, or alternatively the system bandwith of the nominal planning and execution as well as the reflex reaction level. Typically, the former acts at a much lower frequency than the latter one (after [69.86, 140])

control loop of the system. A still relatively open research problem is how to resolve potential failures after reflexes were triggered by planning suitable re-entering and continuation of the task.

69.6.4 Reactive Control Architecture

Obviously, the diverse methods and complex requirements in the pHRI domain and more specifically from interaction control, reflex planning, human-centered motion planning, and interaction planning make new architectural concepts necessary. The central requirements to an according control architecture become rather different from the classical ones (Chap. 12) due to the demands for very responsive behavior not only on control but also on planning level. Figure 69.30 depicts such a reactive control framework [69.167] (VIDEO 616). One of the main questions to address is how to adapt dynamically, safe, and task consistent, while keeping the overall plan and the respective context in mind. The control framework is composed of three layers of abstraction operating at different time scales:

1. On the highest level of abstraction a *global task planning* module builds global task plans that contain temporo-logical concatenations of robot skills, which are derived from any suitable task planning language. Typically, this module runs either offline, in particular when building an entire nominal task plan that contains interaction schemata, or at very slow update rates of several seconds or minutes, depending on the complexity and novelty of the respective task. Skills are topologically invariant capability structures, which instantiations can be modified in terms of skill parameter vectors. The most basic skill is the atomic robot action that represents the formal interface to the robot real-time control core and mechatronics. More complex skills can, e.g., be *grasp an object* or *hand over an object*. Each skill itself is aware of the current task state and which atomic action is currently being executed. This information is then sent to the *dynamic planning layer*.
2. The second layer of abstraction, the *dynamic planning level* is capable of executing and/or modifying plans dynamically, which means that it shall run at least in the range of $\approx 1-10$ Hz. It is responsible

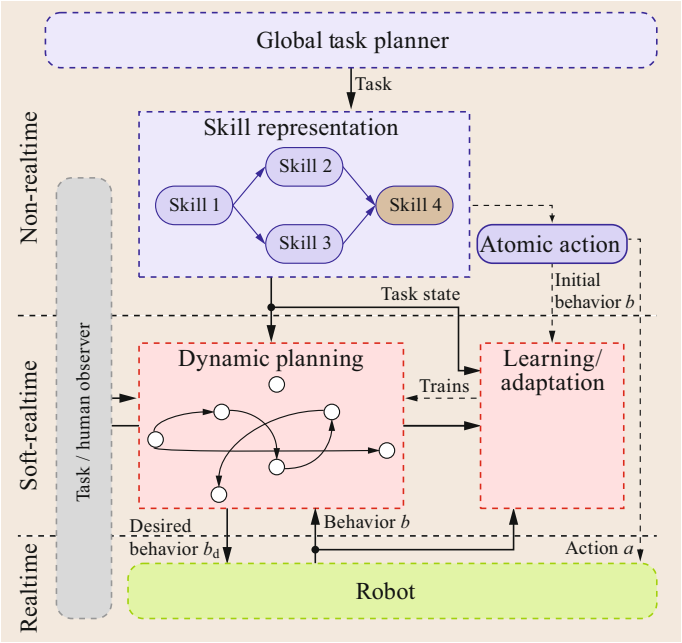

Fig. 69.30 Reactive and human-friendly control framework for acting in partially known environments and interaction ►

for selecting the best action under the premise of the current task state, human state and behavior, as well as the environmental state. In a *learning and adaptation* unit the global task knowledge is translated into the respective dynamic planning domain language, i. e., global knowledge and plans are encoded into a dynamic level such that dynamic adaptation can make use of global context and the respective mission. The according reactive planning unit is then able to (re-)plan the robot's desired nominal actions such that safe, yet task consistent actions, are executed if possible. In particular, instantaneous perception may cause alterations of the original global plans. A major task on this abstraction level is to change the preplanned course of action safely and task consistently. However, finding its way back into the task is at least equally challenging and requires careful treatment (re-entry planning).

3. The lowest architectural layer is the *low-level (real-time) control layer*. Typically, this is subdivided into multiple hierarchical layers, involving also the reflex machine (Fig. 69.29). However, for sake of clarity, we consider it to be a single consistent representation that is accessible via a desired action/behavior complex (a_d, b_d) that is sent to the system for execution. As the desired behavior may alter due to reflex behaviors in case of accidental events such as unforeseen collisions, the control layer feeds back the currently active action/behavior pair (a, b), such that the *dynamic planning layer* is able to react accordingly.

Fundamental to the aforementioned architecture is the capacity to observe human actions on various levels of abstraction. In this sense, a *human observer* that gathers all relevant information and knowledge about human agents is essential. In particular, it provides human-related information that can be of further use.

69.7 Conclusions and Challenges

pHRI has become a central discipline in robotics over the last decade. This is due to the significant progress made in the fields of mechatronics, interaction control, motion planning, and 3-D sensing toward highly integrated and sensorized lightweight systems that are able to physically interact with their surrounding. In direct consequence the learning, planning, and execution of safe and legible interactions has become a widely taken research direction. Clearly, the rise of a new generation of commercial robots capable of physical interaction has also contributed to the large interest in the field. The robotics research and industrial community expects these systems to open up new markets and to push robotics further toward domestic applications that may also involve even more complex and possibly mobile manipulators.

However, despite this recent success in research and also in the commercialization of assistance robots, there are many open research questions that need to be tackled before this class of systems can become a commodity not only in early adopter industrial applications but also on a broader scale: Continuing the road toward safe robotics by tightly coupling injury biomechanics and safe interaction control with lightweight and compliant robot design will further push the boundaries and build the foundation of pHRI. On the other hand, learning interaction controllers and planning intuitive and safe interactions are still very young fields, however, they are the key to solving the long-term physical interaction problem. Furthermore, the current application of assistance robots in real-world problems will bring further novel research questions. The recent

use of these robots clearly underlines that the programming models and paradigms of interaction and soft manipulation are very different from classical industrial robot programming. In particular, they go beyond simple pick and place models toward models of *force based programming*, an interesting research question currently being investigated by various researchers worldwide.

Video-References

VIDEO 606 Mobile robot helper – Mr. Helper
available from http://handbookofrobotics.org/view-chapter/69/videodetails/606

VIDEO 607 Generation of human care behaviors by human-interactive robot RI-MAN
available from http://handbookofrobotics.org/view-chapter/69/videodetails/607

VIDEO 608 Injury evaluation of human-robot impacts
available from http://handbookofrobotics.org/view-chapter/69/videodetails/608

VIDEO 609 Safe physical human-robot collaboration
available from http://handbookofrobotics.org/view-chapter/69/videodetails/609

VIDEO 610 Admittance control of a human centered 3 DOF robotic arm using differential elastic actuators
available from http://handbookofrobotics.org/view-chapter/69/videodetails/610

VIDEO 611 A control strategy for human-friendly robots
available from http://handbookofrobotics.org/view-chapter/69/videodetails/611

VIDEO 613 Human–robot interactions
available from http://handbookofrobotics.org/view-chapter/69/videodetails/613

VIDEO 614 ISAC: A demonstration
available from http://handbookofrobotics.org/view-chapter/69/videodetails/614

VIDEO 615 Smart fur
available from http://handbookofrobotics.org/view-chapter/69/videodetails/615

VIDEO 616 Human–robot interaction planning
available from http://handbookofrobotics.org/view-chapter/69/videodetails/616

VIDEO 617 The power of prediction: Robots that read intentions
available from http://handbookofrobotics.org/view-chapter/69/videodetails/617

VIDEO 618 Reach and grasp by people with tetraplegia using a neurally controlled robotic arm
available from http://handbookofrobotics.org/view-chapter/69/videodetails/618

VIDEO 619 An assistive decision and control architecture for force-sensitive hand–arm systems driven via human–machine interfaces (MM1)
available from http://handbookofrobotics.org/view-chapter/69/videodetails/619

VIDEO 620 An assistive decision and control architecture for force-sensitive hand–arm systems driven via human–machine interfaces (MM2)
available from http://handbookofrobotics.org/view-chapter/69/videodetails/620

VIDEO 621 An assistive decision-and-control architecture for force-sensitive hand–arm systems driven by human–machine interfaces (MM3)
available from http://handbookofrobotics.org/view-chapter/69/videodetails/621

VIDEO 622 An assistive decision-and-control architecture for force-sensitive hand–arm systems driven by human–machine interfaces (MM4)
available from http://handbookofrobotics.org/view-chapter/69/videodetails/622

VIDEO 623 Twendy One demo
available from http://handbookofrobotics.org/view-chapter/69/videodetails/623

VIDEO 624 Full body compliant humanoid COMAN
available from http://handbookofrobotics.org/view-chapter/69/videodetails/624

VIDEO 625 Physical human–robot interaction in imitation learning
available from http://handbookofrobotics.org/view-chapter/69/videodetails/625

VIDEO 626 Justin: A humanoid upper body system for two-handed manipulation experiments
available from http://handbookofrobotics.org/view-chapter/69/videodetails/626

VIDEO 627 Torque control for teaching peg in hole via physical human–robot interaction
available from http://handbookofrobotics.org/view-chapter/69/videodetails/627

VIDEO 632 Flexible robot gripper for KUKA Light Weight Robot (LWR): Collaboration between human and robot
available from http://handbookofrobotics.org/view-chapter/69/videodetails/632

VIDEO 716 Human–robot handover
available from http://handbookofrobotics.org/view-chapter/69/videodetails/716